



funded by the European Union

Awareness and resilience through European multi sensor system

D2.5– Report of hydrogeology of the selected areas

Version 1 15/05/2023

Disclaimer

Funded by the European Union. Views and opinions expressed are however those of the author(s) only and do not necessarily reflect those of the European Union or of the European Commission-Euratom. Neither the European Union nor the granting authority can be held responsible for them.

While this document has been prepared with care, the authors and their employers provide no warranty concerning the content and shall not be liable for any direct, incidental or consequential damages that may result from the use of the information or the data contained in it. Reproduction is authorised provided the material is unabridged and the source is acknowledged.

Document type	Deliverable
Document number	D2.5 version 1
Document title	Report of hydrogeology of the selected areas
Authors	Marino Domenico Barberio, Vincenzo Guerriero, Vasileios Karakostas, Christos Kourouklas, Eleftheria Papadimitriou, Luca Pizzino, Stylianos Stoulos, Michael Strupler, Marco Tallini
Release date	15/05/2023
Contributing partners	AuTh, ETH, INGV, UNIVAQ
Dissemination level	Public

Version	Short description	Main authors	Coordinator
1	First release	Marino Domenico Barberio, INGV Vincenzo Guerriero, UNIVAQ Vasileios Karakostas, AuTh Christos Kourouklas, AuTh Eleftheria Papadimitriou, AuTh Luca Pizzino, INGV Stylianos Stoulos, AuTh Michael Strupler, ETH Marco Tallini, UNIVAQ 15.5.2023	Ayse Nyberg, KTH

Abstract

The present document is a review of the hydrogeology of the three selected areas in which, within the artEmis project, the potential groundwater sites for radon monitoring will be located.

The selected areas are the Abruzzi region (Italy), the Ionian Islands and the Gulf of Corinth (Greece) and Bedretto lab and Swiss Alps.

Within the artEmis project, the Abruzzi region (Italy) has been managed by UNIVAQ and INGV, the Ionian islands and the Gulf of Corinth (Greece) by AuTh, and Bedretto lab and Swiss Alps by ETH.

Table of contents

Disclaimer	2
Abstract	3
Table of contents.....	4
1 Introduction.....	5
1.1 References.....	6
2 Hydrogeology of the Abruzzi region (Italy).....	6
2.1 The carbonate ridges.....	6
2.2 The terrigenous hilly and mountainous areas.....	14
2.3 The intermontane plains and the fluvial plains.....	15
2.4 Earthquake hydrology	16
2.4.1 Introduction.....	16
2.4.2 Earthquake hydrology of Abruzzi region	17
2.5 References.....	21
3 Hydrogeology of the Ionian Islands and the Gulf of Corinth (Greece)	24
3.1 Hydrogeology of central Ionian islands	24
3.1.1 Hydrogeology of Lefkada island.....	24
3.1.2 Hydrogeology of Kefalonia island	26
3.2 Hydrogeology of Gulf of Corinth	30
3.3 References	34
4 Hydrogeology of Bedretto lab and Swiss Alps	36
4.1 Hydrogeology of the Swiss Alps.....	36
4.2 Hydrogeology of the Bedretto site.....	37
4.3 References.....	38

1 Introduction

Many studies showed that several geogas and hydrogeochemical parameters of groundwater changed during pre- and post-seismic phases of an earthquake. Radon, which is nowadays viewed as an efficient tracer of the geodynamic processes occurring in the Earth's crust, is included among these parameters. Radon is even considered a potential earthquake precursor due to its changes anticipating the seismic event (Kawabata et al., 2020 and references therein; Morales-Simfors et al., 2020 and references therein; Wakita et al., 1980). Thus, radon amount measurements in groundwater could help to understand the crustal deformation processes such as crack enucleation or strain changes, which enhance before the earthquake occurrence (Asano et al., 2001). Considering the premise, within the artEmis project, a multiparametric up-to-date low-cost sensors network will monitor radon in groundwater with a remarkable spatial and temporal resolution in three European areas selected on the base of their significant seismicity and peculiar seismotectonic, geological and hydrogeological setting, but also for having a quite efficient logistic background. The final goal of the artEmis project is to use the radon monitoring in groundwater as a potential seismic precursor. Therefore, particular attention, in this first step of the artEmis project, will be given to the selection of the radon monitoring sites in the three areas which should be possibly hydro- or geogas-sensitive in response to the seismic activity (Gori and Barberio, 2022). The location of these sites is based on the knowledge of the physical properties of source rocks, the hydrogeological setting, the seismotectonic background and the seismic activity, since radon release in groundwater depend on them (Kawabata et al., 2020 and references therein). These topics are described in detail in the deliverables D2.1-D2.6. The present deliverable concerns on the description of the hydrogeology of the three selected areas (Abruzzi region, Italy; Ionian Islands and Gulf of Corinth, Greece; Bedretto lab and Swiss Alps) (fig. 1.1). The Abruzzi region (Italy) has been managed by UNIVAQ and INGV, the Ionian islands and the Gulf of Corinth (Greece) by AUTH, and Bedretto lab and Swiss Alps by ETH.

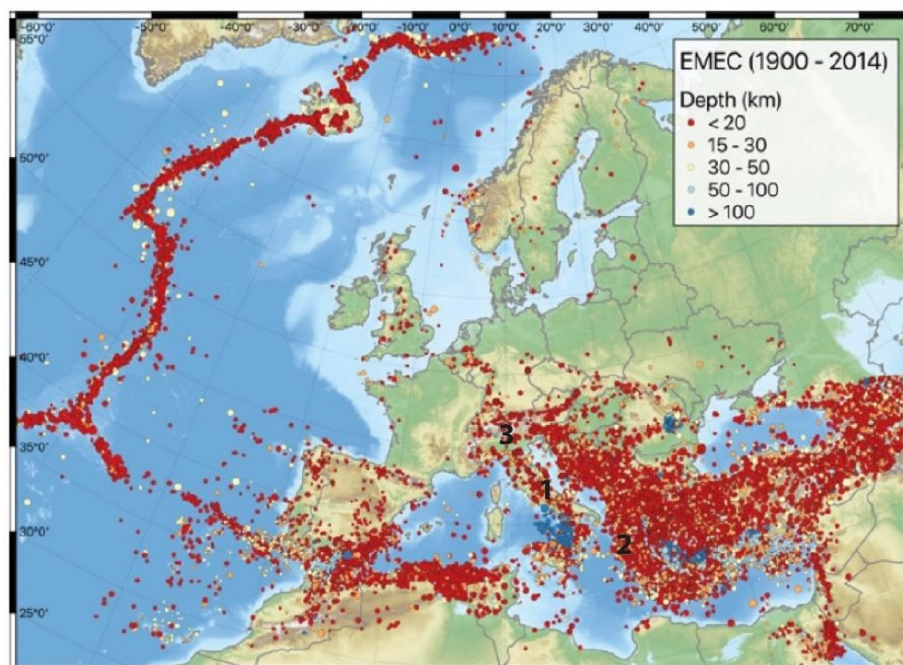


Figure 1.1: The complete European-Mediterranean earthquake catalogue (EMEC) for the period 1900 – 2012 by Danciu et al. (2021) with the location of the three selected areas (1: Abruzzi region, Italy; 2: Ionian Islands and Gulph of Corinth, Greece; 3: Bedretto lab and Swiss Alps)

1.1 References

- Asano, T., Sato, K., Onodera, J. I., 2001. United nations scientific committee on the effects of atomic radiation 2000 report. Japanese Journal of Health Physics 36(2), 149-158. <https://doi.org/10.5453/jhps.36.149>
- Danciu, L., Nandan, S., Reyes, C., Basili, R., Weatherill, G., Beauval, C., Rovida, A., Vilanova, S., Sesetyan, K., Bard, P.-Y., Cotton F., Wiemer, S., Giardini, D., 2021. The 2020 update of the European Seismic Hazard Model: Model Overview. EFEHR Technical Report 001, v1.0.0. <https://doi.org/10.12686/a15>
- Gori, F., Barberio, M. D., 2022. Hydrogeochemical changes before and during the 2019 Benevento seismic swarm in central-southern Italy. Journal of Hydrology 604, 127250. <https://doi.org/10.1016/j.jhydrol.2021.127250>
- Kawabata, K., Sato, T., Takahashi, H. A., Tsunomori, F., Hosono, T., Takahashi, M., Kitamura, Y., 2020. Changes in groundwater radon concentrations caused by the 2016 Kumamoto earthquake. Journal of Hydrology 584, 124712. <https://doi.org/10.1016/j.jhydrol.2020.124712>
- Morales-Simfors, N., Wyss, R. A., Bundschuh, J., 2020. Recent progress in radon-based monitoring as seismic and volcanic precursor: A critical review. Critical reviews in environmental science and technology 50(10), 979-1012. <https://doi.org/10.1080/10643389.2019.1642833>
- Wakita, H., Nakamura, Y., Notsu, K., Noguchi, M., Asada, T., 1980. Radon anomaly: a possible precursor of the 1978 Izu-Oshima-kinkai earthquake. Science 207(4433), 882-883. [DOI: 10.1126/science.207.4433.882](https://doi.org/10.1126/science.207.4433.882)

2 Hydrogeology of the Abruzzi region (Italy)

The groundwater resources of the Abruzzi region, considering the permeability values of the sedimentary units, are located in four main different geological & geomorphological environments: the carbonate ridges and the intermontane plains, placed above all in L'Aquila district, the terrigenous hilly and mountainous areas, which include both the Mts. Laga (Teramo district) and the periadriatic hilly areas (Pescara and Chieti districts), and the fluvial plains (figs. 2.1 and 2.2) (Petitta et al., 2003).

The amount of the water resources of the Abruzzi region can be estimated by considering the sum of the contributions of the rivers to the sea, on average equal to about 4,000 million m³/year. This contribution includes both runoff waters and groundwater from punctual and linear springs. The overall flow of springs and runoff waters can be estimated as at least 60% of the total water resources (Petitta et al., 2003).

The two outflow rates have very different characteristics. The runoff waters have a regime directly dependent on the rainfall and are, therefore, concentrated in the rainy months, of poorer quality, suitable for industrial, hydroelectric and, to a lesser extent, irrigation uses.

The base groundwater flow, conversely, has a seasonal regularity of outflow and supports the water flow of rivers during the dry periods, has high quality parameters, such as to guarantee optimal use of drinking water or irrigation (Petitta et al., 2003).

2.1 The carbonate ridges

The carbonate ridges are composed of Meso-Cenozoic carbonate rocks (mainly limestone, dolomite and, in the northern and eastern part of the Abruzzi region by marly-cherty limestone) and represent the main aquifers where the precipitations chiefly feed the infiltration towards the subsoil (figs. 2.2, 2.3, 2.4). In the carbonate aquifer, groundwater flowpaths are conditioned by many parameters (tectonic setting, fracture network, evolution of karst features, unsaturated zone, local recharge effects, lithological setting nearby the springs, etc.). All these factors affect, at regional and local scale, groundwater hydrodynamics, flowpaths and

hydrochemistry and causing the distribution of water resources (Adinolfi Falcone et al., 2008; Boni et al., 2000; Barbieri et al., 2005; Petitta and Tallini, 2002). Groundwater flows through the fracture network and the shallow and underground karst features (e.g., doline field, polje, karst cave) to reach the saturated zone. The aquifers host generally a unique regional wide groundwater table (hydraulic gradient: 5-20 per thousand) which is sometimes displaced by faults acting as low-permeability barrier. In other cases, the faults can act as drain, favouring the groundwater anisotropic flowing along the fault plane. Each fissured-karst carbonate ridge, surrounded at its periphery by low-medium permeability rocks, acts as an independent hydrogeological structure and the aquifer outcropping area consists of its recharge zone (Boni, 2000). The low and medium permeability rocks correspond to the Miocene regional terrigenous units (regional aquiclude) and the Quaternary detrital lithologies filling up the intermontane plains (local aquitards), respectively.

The main springs are placed at the periphery of the carbonate massifs, generally along the contact with the less permeable formations, such as mainly the Miocene terrigenous lithologies (regional aquiclude). The main springs have a very high discharge (from a few hundred to several thousand liters per second) which is, as a rule, stable over time, with slight seasonal fluctuations, testifying the large recharge area of the carbonate aquifers.

As concerns the karst features, most probably, a deep karst network developed in the Quaternary times (2.5 Myr) at lower altitudes than those of today's main springs. Afterwards the filling of the intermontane basins by detrital deposits blocked the springs of this paleokarst network and conditioned an upward rising of the spring altitude to their present position (Boni, 2000). This hypothesis is suggested by the following evidence: (i) most of the principal springs are placed at the border of the intermontane basins filled by Quaternary detrital deposits; (ii) the geomorphology around the principal springs is still young and immature, since karst water does not emerge from a single karst conduit but, conversely, outflows through several small springs located over a quite large area (about several square kilometres); (iii) the principal karst springs with a great discharge values of about several m^3/s show a steady discharge regime with maximum and minimum fluctuations not overcoming the 50% of the mean discharge.

In the following the carbonate aquifers and the main springs of Abruzzi region are outlined (figs. 2.2-2.5). The springs described in the text are reported with a numbering in fig. 2.3.

The chief representative carbonate aquifer of Abruzzi is the Gran Sasso aquifer which is very large with an area of about $1,000 \text{ km}^2$ (figs. 2.2-2.5). The groundwater flows with a radial pattern from its preferential recharge area (concentrated at the core of the aquifer, at the Campo Imperatore high plain) to the springs located above all along in its periphery (Petitta and Tallini, 2022; Scozzafava and Tallini, 2001). It is drained by low-altitude springs located mostly on the southern slope, in the L'Aquila area (Vetoio and Boschetto: 1, Vera and Tempera: 2) (total discharge about $2 \text{ m}^3/\text{s}$) and in the Tirino R. valley (Capodacqua, 3; Presciano, 4; Basso Tirino, 5) (total discharge about $12 \text{ m}^3/\text{s}$). In L'Aquila area the springs outflow through the groundwater transfer from the carbonate aquifer toward the Quaternary detrital deposits of L'Aquila intermontane plain (Vetoio and Boschetto springs). Vera and Tempera springs originate possibly for the direct flowing toward south, facilitated also by karst features, from the main recharge area (Campo Imperatore) toward L'Aquila plain. The springs of the Tirino R. valley are caused conversely by the intersection between the heavily incised valley of Tirino R. with the regional water table. At the southern edge of the aquifer, near Popoli, the S. Calisto spring (6, discharge: $2 \text{ m}^3/\text{s}$) and a contribution to the important spring of Capo Pescara are worth mentioning.

On the northern side, high-altitude spring groups (Chiarino, 7; Rio Arno, 8; Ruzzo, 9; Vitella d'Oro and Mortaio d'Angri, 10, total discharge about $1 \text{ m}^3/\text{s}$) are placed along the overthrust which causes the superposition of carbonate rocks (regional aquifer) onto the terrigenous ones (regional aquiclude) and representing hydrogeologically a significant permeability boundary. Finally, to the "natural" springs, the "artificial"

groundwater drainage of the Gran Sasso highway tunnels (southern drainage: 11; northern drainage: 12) (total discharge about 1.5 m³/s) must be added. Groundwater of the high-altitude spring groups and the Gran Sasso tunnels drainage is withdrawn for drinkable water purposes.

The Capo Pescara spring (13) at Popoli, with a discharge of about 7 m³/s, is the largest spring in Abruzzi. It is located in the lowest discharge area of Gran Sasso and Sirente aquifers, drawing its nourishment from the two aquifers.

The springs of Molina Aterno and the drainage in the middle Aterno R. valley (14) are also fed by the Sirente aquifer (total discharge: 1-1.5 m³/s), the Fontana Grande spring (15) in Celano (discharge: 0.3 m³/s) and the Raiano spring (16) (discharge: 2 m³/s) fed by the Prezza Mt. aquifer.

The Velino Mt. – Nuria Mt. aquifer feeds springs located in the Lazio region, relating to the Peschiera-Velino R. valley spring group (17) (total discharge: 30 m³/s), partially exploited for the drinking water supply of the city of Rome. A smaller groundwater quantity flows towards the northern edge of the Fucino plain (discharge: 1 m³/s).

The Western Marsica aquifer are mainly drained by the Posta Fibreno spring (18) (discharge: 10 m³/s), but part of the groundwater flows towards the Fucino plain, and part towards the Trasacco, Ortucchio and Venere springs (19) (discharge: 4 m³/s), whose discharge is strongly influenced by many well fields.



Figure 2.1: Abruzzi region (central Italy)

(https://it.wikipedia.org/wiki/Abruzzo#/media/File:Cartina_fisica_Abruzzo_2019.png)

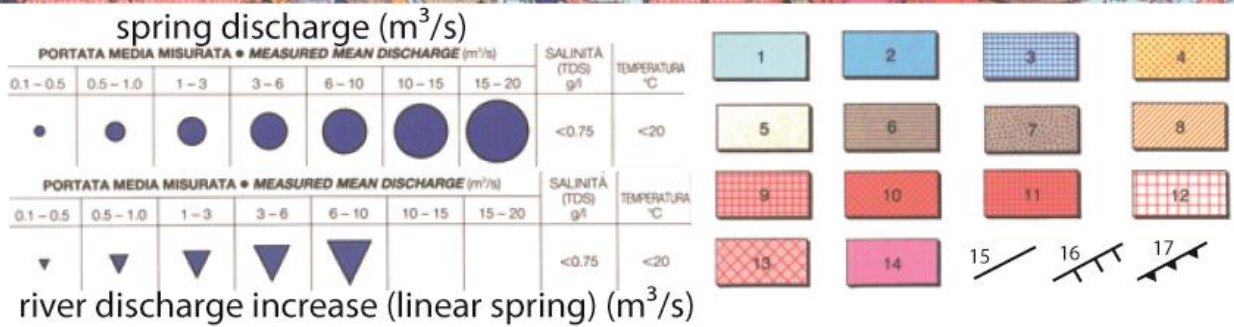
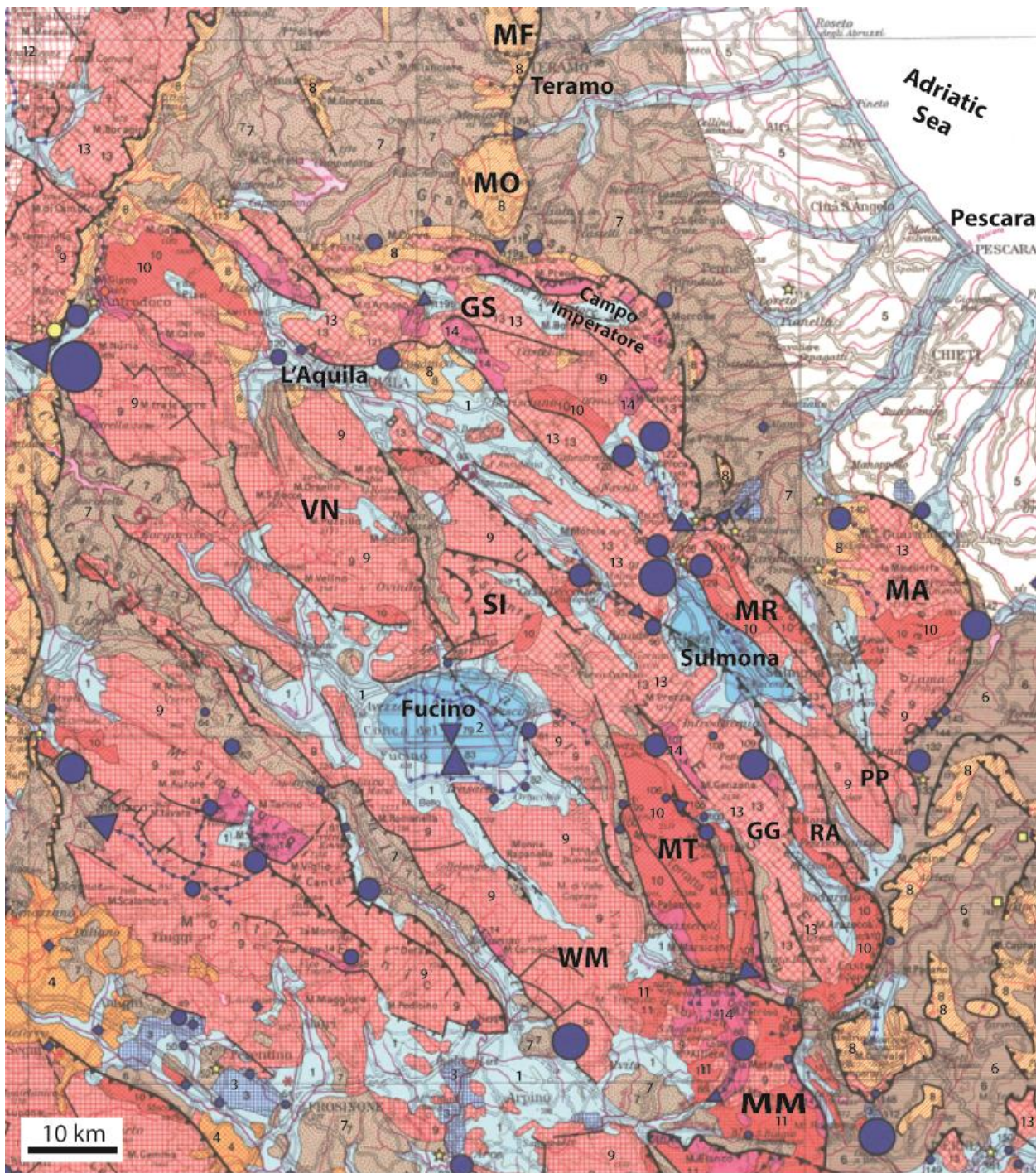


Figure 2.2

Figure 2.2 (caption of figure 2.2, previous page): Hydrogeological scheme of Abruzzi region (from Boni et al., 1986). Main carbonate aquifer: MF: Montagna dei Fiori; MO: Montagnone; GS: Gran Sasso; VN: Velino Mt.-Nuria Mt.; SI: Sirente Mt.; MR: Morrone Mt.-Roccatagliata; MA: Maiella; MT: Montagna Grande-Terratta; GG: Genzano Mt.-Greco Mt.; RA: Rotella Mt.-Arazecca Mt.; PP: Pizzalto Mt.-Porrara Mt.; WM: Western Marsica; MM: Meta-Mainarde. Hydrogeological complexes: 1: alluvial detrital deposits with limited thickness (gravel, sand, silt, clay), Pleistocene-Holocene (mono- and multi-layer aquifer); 2: continental (alluvial, lacustrine, slope) detrital deposits of the intermontane plains with remarkable thickness (gravel, sand, silt, clay), Plio-Quaternary (multi-layer aquifer); 3: travertines, Quaternary (local aquifer); 4: volcanics (lava and tuff), Plio-Quaternary (multi-layer aquifer); 5: marine clay, Plio-Pleistocene (regional aquiclude); 6: clayey “flysch” with lithoid intercalations (sandstone, marl, limestone), Miocene-Cretaceous (regional aquiclude); 7: arenaceous-pelitic “flysch” (terrigenous turbidites), Lower Pliocene-Late Miocene (regional aquiclude); 8: marl and calcarenite, Miocene (local aquifers, regional aquitard-aquiclude); 9: limestone and dolomitic limestone belonging to the Lazio-Abruzzi Meso-Cenozoic shallow-water carbonate platform (regional aquifer); 10: detrital and reef limestone belonging to the edge lithofacies of the Lazio-Abruzzi carbonate platform, Cretaceous-Jurassic (regional aquifer); 11: detrital limestone and breccia belonging to slope to basin and ramp lithofacies of the Lazio-Abruzzi carbonate platform, Paleogene-Jurassic (regional aquifer); 12: marly-calcareous-cherty lithologies belonging to the Umbria-Marche-Sabina deep-water pelagic basin, Oligocene-Jurassic (regional multilayer aquifer); 13: detrital limestone with marls and cherts belonging to the transitional (slope to basin) lithofacies between the Lazio-Abruzzi carbonate platform and the Umbria-Marche-Sabina pelagic basin, Oligocene-Jurassic (regional multilayer aquifer); 14: basal dolomites, lower Liassic-Upper Triassic (regional aquiclude-aquitard); 15: undefined faults; 16: extensional faults; 17: thrust

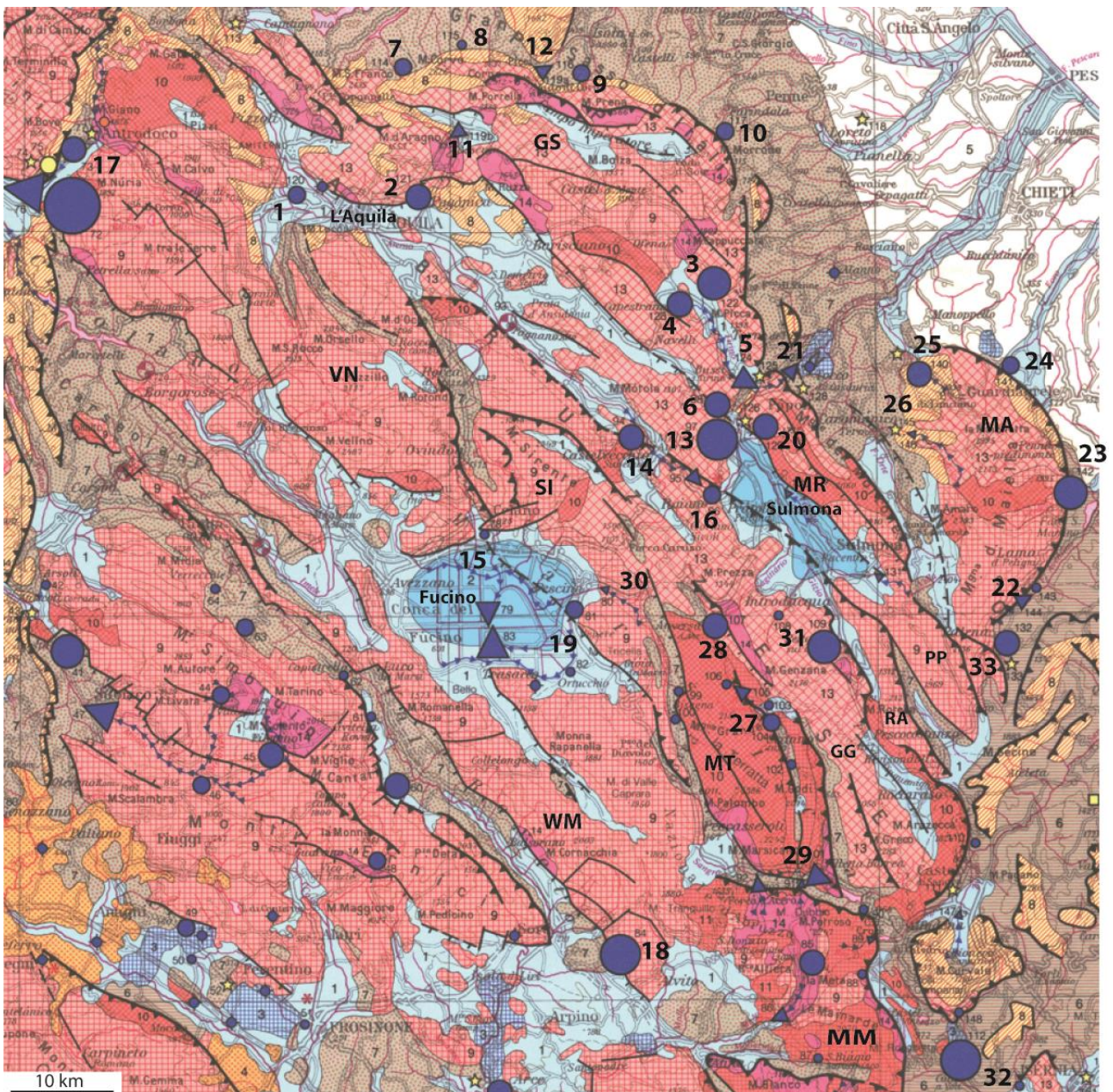


Figure 2.3: Hydrogeological scheme of Abruzzi region with the location of the main springs described in the text (from Boni et al., 1986). Main carbonate aquifer: MF: Montagna dei Fiori; MO: Montagnone; GS: Gran Sasso; VN: Velino Mt.-Nuria Mt.; SI: Sirente Mt.; MR: Morrone Mt.-Roccatagliata; MA: Maiella; MT: Montagna Grande-Terrata; GG: Genzano Mt.-Greco Mt.; RA: Rotella Mt.-Arazeca Mt.; PP: Pizzalto Mt.-Porrara Mt.; WM: Western Marsica; MM: Meta-Mainarde. Springs: 1- Vetoio and Boschetto; 2: Vera and Tempera; 3: Capodacqua; 4: Pesciano; 5: Tirino R. linear spring; 6: S. Calisto; 7: Chiarino; 8: Rio Arno; 9: Ruzzo; 10: Mortaio d'Angri and Vitella d'Oro; 11: southern Gran Sasso tunnels drainage; 12: northern Gran Sasso tunnels drainage; 13: Capo Pescara; 14: Molina Aterno; 15: Fontana Grande; 16: Raiano; 17: Peschiera; 18: Posta Fibreno; 19: Trasacco, Ortucchio and Venere; 20: Giardino; 21: Pescara R. linear spring; 22: S. Giustino and Acquevive; 23: Verde; 24: Foro; 25: Lavinio; 26: Orfento R. linear spring; 27: Villalago; 28: Cauto; 29: Villetta Barrea; 30: Giovenco linear spring; 31: Gizio; 32: Capo Volturno; 33: Capodifiume Aventino

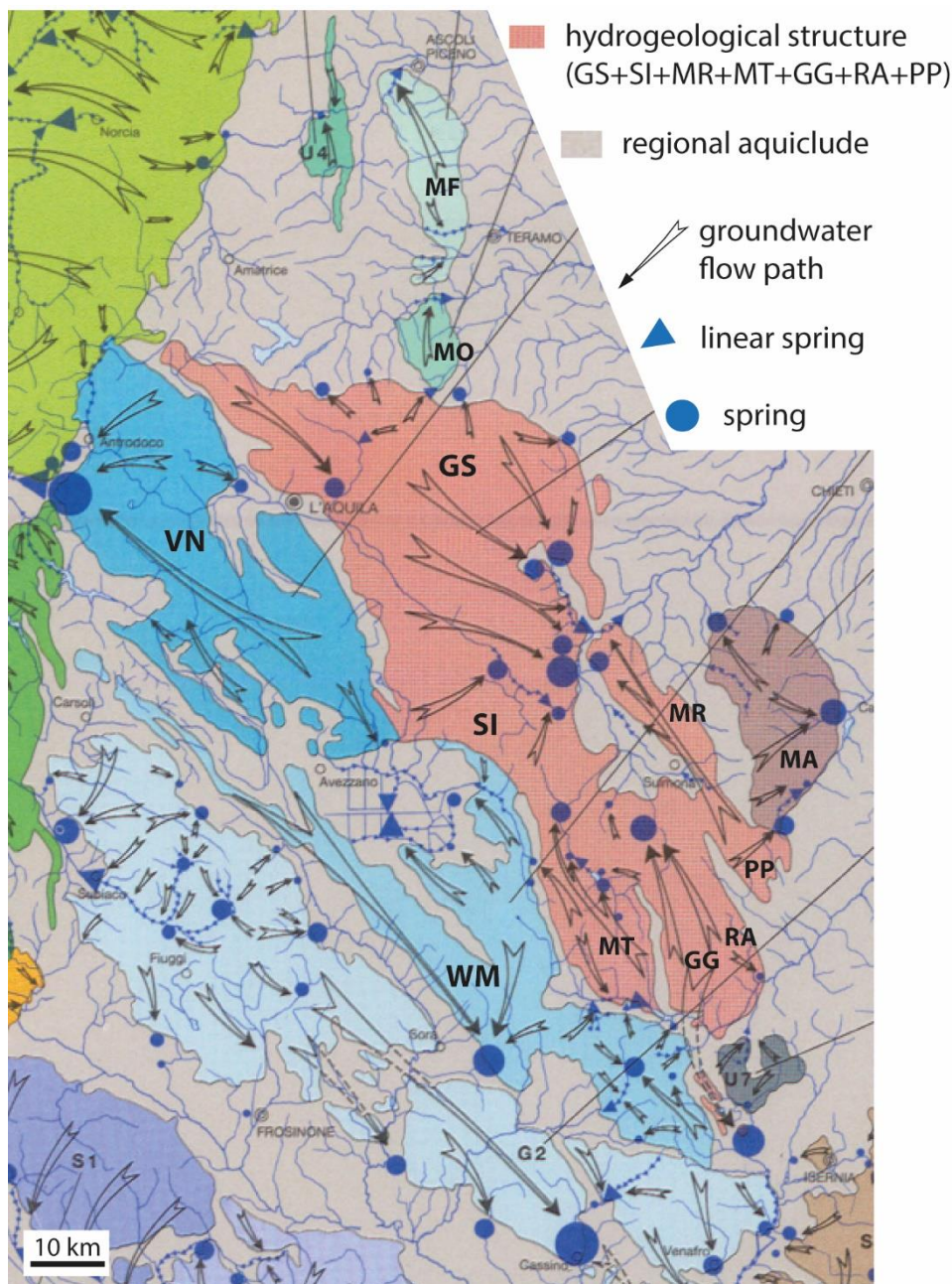


Figure 2.4: The main carbonate hydrogeological structures of Abruzzi region and the regional groundwater flow paths (from Boni et al., 1986). MF: Montagna dei Fiori; MO: Montagnone; VN: Velino Mt.-Nuria Mt.; WM: Western Marsica; MA: Maiella; The following aquifers refer to a unique hydrogeological structure: Gran Sasso (GS); Sirente Mt. (SI); Morrone Mt.-Roccatagliata (MR); Montagna Grande-Terratta (MT); Genzano Mt.-Greco Mt. (GG); Rotella Mt.-Arazzecca Mt. (RA); Pizzalto Mt.-Porrara Mt. (PP)

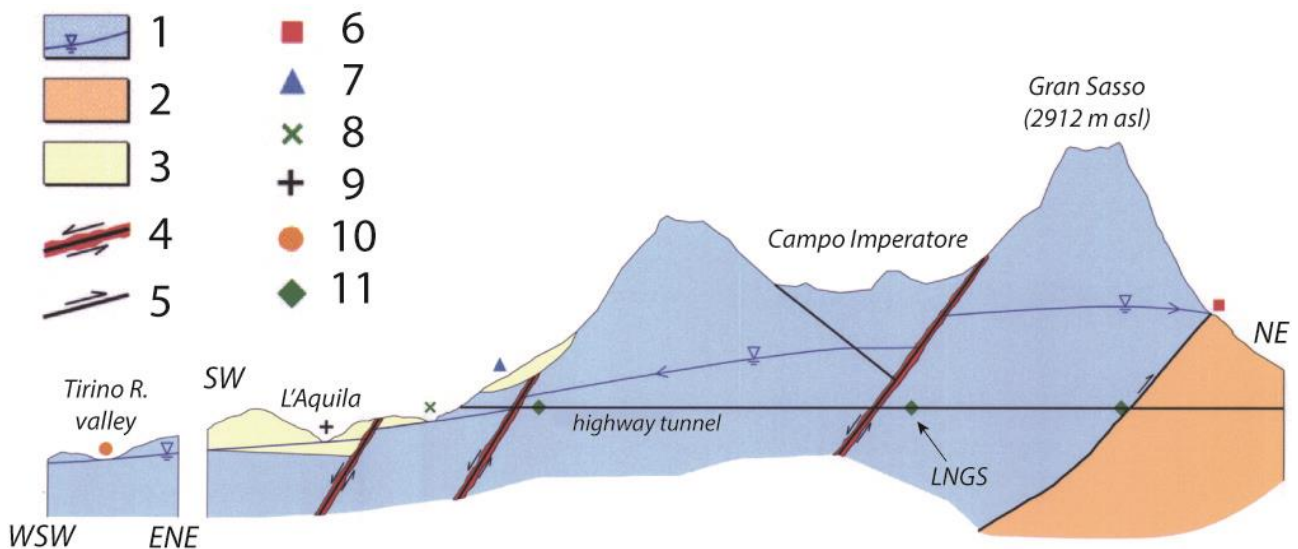


Figure 2.5: Gran Sasso aquifer schematic section with the location of the main spring groups (not in scale) (from Petitta and Tallini, 2002). 1: carbonate aquifer, the blue line refers to the water table; 2: regional terrigenous aquiclude (sandstone and pelite); 3: aquitard (detrital deposit of intermontane plains); 4: fault with fault rock (low-permeability barrier); 5: regional thrust (permeability boundary); spring group: 6: high-altitude outflow spring (northern slope); 7: local high-altitude spring fed by perched aquifer; 8: spring fed by groundwater flowing into karst features (?) and due to regional water table outcropping; 9: spring due to regional water table outcropping 10: low-altitude spring due to regional water table outcropping (linear and punctual spring); 11: highway tunnels drainage. LNGS: Gran Sasso underground Nuclear Physics laboratory

The Morrone Mt.-Roccatagliata aquifer is drained by the Giardino spring (20) (discharge: 1 m³/s), exploited for drinking water purposes, and by the Pescara R., when it crosses the Popoli gorges (21) (discharge: 0.7 m³/s). The aquifer subordinately feeds also the Sulmona alluvial multilayer aquifer, through the alluvial fans of the western slope.

The Maiella aquifer is drained essentially on the eastern slopes, through the stratigraphic and tectonic boundaries with the Pliocene fine-grained deposits, and in the NE slope in correspondence with tectonic alignments. The main discharge areas, from S to N, are as follows: the S. Giustino spring (discharge: 0.6 m³/s) which directly feeds the Aventino River; the Acquevie linear spring (total discharge: 1 m³/s) along the Aventino R. (22); the Verde spring (23) (discharge: 2.6 m³/s) which represents the major discharge of the aquifer, as well as the main drinking water resource of the Chieti district; the Foro spring (24) (discharge: 0.6 m³/s), fully exploited; the Lavinio spring (25) (discharge: 1.8 m³/s) enriched in sulphates for the groundwater flowing within evaporite lithologies (mainly gypsum). The unique discharge area of the basal aquifer on the western side is the Orfento R. which, between 480 and 405 meters asl, undergoes an average discharge increase of about 0.15 m³/s (26, linear spring).

The Montagna Grande-Terratta aquifer mainly feeds the Tasso-Sagittario basin, with the springs of Villalago (27) (discharge: 2.4 m³/s) and those of the Cauto (28) (discharge: 1.7 m/s). Other springs are located along the Sangro River in Villetta Barrea, with the linear springs of Villetta Barrea (29) (discharge: 1.4 m³/s) and in the Giovenco R. valley (30) (discharge: 0.6 m³/s).

The Genzana Mt.- Greco Mt. aquifer is drained to the N by the Gizio spring (31) (discharge: 2.2 m³/s), located on the edge of the Sulmona plain, while in the southern sector of this aquifer contributes with about 3 m³/s, to half of the notable discharge of the Capo Volturmo spring (discharge: 6 m³/s) (32).

The Pizzalto Mt. -Porrara Mt. aquifer is tectonically separated from the neighbouring Rotella Mt. - Arazzecca Mt. aquifer. The Pizzalto-Porrara aquifer feeds the discharge of the Capodifiume Aventino spring (33) located on the south-eastern edge with about 1.8 m³/s. The Rotella Mt. – Arazzecca Mt. aquifer contributes, instead, with about 2.1 m³/s to feed the Capo Volturno spring (32) together with the Genzana Mt. - Greco Mt. aquifer (see above).

The Meta-Mainarde Mts. aquifer is characterized by groundwater circulation conditioned by the abundant presence of dolomite, which facilitates the drainage into the rivers (linear springs) and the feeding of springs located in correspondence with faults. Part of the hydrostructure drains towards the Sangro River to the N, part towards the Melfa River in Lazio and part towards the Volturno R. basin to the SE.

The total mean discharge of the main aquifers of Abruzzi region as reported by Petitta et al. (2003) is about 98.5 m³/s for a total recharge area of about 4500 km² (tab. 2.1, fig. 2.4). Therefore, the mean effective infiltration rate can be calculated following the above-mentioned data in about 690 mm/year. It is a high value typical for the Italian carbonate aquifers.

2.2 The terrigenous hilly and mountainous areas

The terrigenous lithologies (sandstone, mudstone and marly lithologies), mainly Miocene in age, encircled the carbonate ridges and are placed normally at their NE slope via overthrust boundary. They are generally considered to be scarcely permeable, so representing the regional aquiclude with respect to the carbonate aquifers (fig. 2.2).

But, in several cases, these terrigenous lithologies are composed also by arenaceous intervals with subordinate pelites and calcarenitic horizons with rare and thin marly intercalations (e.g. the arenaceous bodies of Laga Mts.). These specific lithological sequences are characterized by not negligible permeability, due above all to the fissure network. Anyway, the groundwater quantities flowing within them is clearly lower than those flowing into the carbonate aquifers, but still worthy of consideration, so constituting one of the main resources for the drinkable water supply of numerous villages.

Carbonate aquifer	Mean discharge (m ³ /s)
Nuria Mt. - Velino Mt.	31
Gran Sasso	20.5
Western Marsica	14.6
Sirente	7.3
Maiella	6.8
Montagna Grande-Terratta	5.5
Genzana Mt.-Greco Mt.	5.2
Pizzalto Mt.-Porrara Mt.	1.8
Morrone-Roccatagliata	1.7
Montagna dei Fiori	1.5
Montagnone	0.5
Total aquifers	98.5

Table 2.1: Estimation of the groundwater resources of the main carbonate aquifers of Abruzzi region and neighbouring areas (Petitta et al., 2003)

2.3 The intermontane plains and the fluvial plains

The intermontane plains have peculiar hydrogeological characteristics and generally host significant groundwater resources. L'Aquila, Fucino and Sulmona plains are the largest ones, but there are also many other minor plains (Campo Imperatore, Montereale, etc.) (fig. 2.2).

The intermontane plains correspond tectonically to half graben or complex graben bounded by mainly SW-dipping extensional faults which acted from Upper Pliocene (3.6 Myr) till now. Many of these faults are also seismogenic. As sedimentological traps, the plains were filled up by Plio-Quaternary chiefly lacustrine, alluvial and slope deposits which act hydrogeologically as a multilayer aquifer.

Coarse-grained slope and alluvial fan deposits are located along the plain borders and are interdigitated also in depth with the plain deposits. The carbonate aquifers and the upper Miocene terrigenous aquiclude encircle the multilayer aquifer of the plains and are placed also below them, forming their substratum.

The groundwater stored in the multilayer aquifer is due to the zenithal recharge (i.e. rainfall falling within the aquifer recharge area), with a limited potential, and to the groundwater transfer from the carbonate aquifers encircling the plains towards the plain multilayer aquifer. In fact, in many cases this such groundwater transfer is recognised, and it occurs through the above-mentioned coarse-grained bodies which show medium-high permeability. It follows that the main springs, showing a significant discharge of several hundred liters per second, are located on the edge of the plains, near the boundary with the carbonate aquifers.

Moreover, groundwater direct contributions to the discharge of rivers flowing in the plains are also frequent, so that the rivers can act as linear springs. Even if the hydrostructure is multilayer, water table measurements show in many cases a single piezometric level which would suggest a hydraulic communication between the different perched local aquifers and the isopiezometric lines indicates a centripetal drainage toward the intermontane plain. In figure 2.6 the hydrogeological scheme of L'Aquila plain, as emblematic intermontane basin of the Abruzzi region, is reported.

The alluvial aquifers located in the fluvial plains have similar hydrogeological characteristics, which differ individually according to the permeability and the thickness of the alluvial deposits (fig. 2.2). In the upper part of the fluvial plains the deposit thickness does not exceed 20 m and gravel lenses and horizons predominate.

The fine-grained sediments are not very thick and discontinuous and so do not prevent the hydraulic contact between the gravel bodies. Therefore, the alluvial deposits can be roughly classified hydraulically as a monolayer aquifer.

Different settings are recognised in the lower part of the fluvial plains. In the fluvial plains of the main rivers, such as the Vomano R., Pescara R. and Sangro R., the location of extensive and thick bodies of fine-grained deposits determines the isolation of gravel and gravel-sandy lenses, giving to the aquifers a multilayer behaviour.

Conversely, monolayer conditions exist in the fluvial plains of the minor rivers, even if lenses of fine-grained horizons separate vertically the gravel bodies, sometimes identifying perched aquifers.

All the alluvial aquifers lay on aquiclude such as the Plio-Pleistocene clayey low permeability sediments and subordinately by Late Miocene terrigenous units.

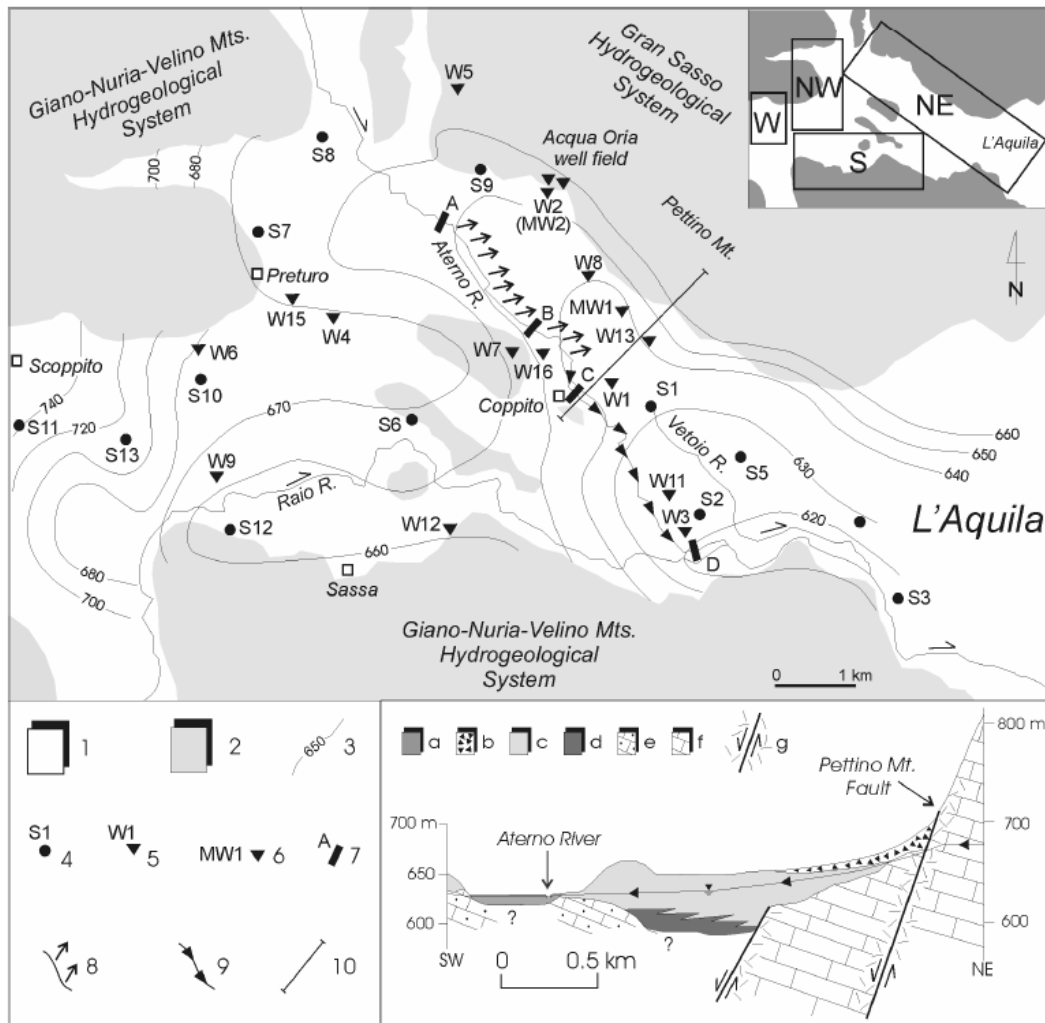


Figure 2.6: Hydrogeological setting of the Pettino Mt.-Aterno R. area (L'Aquila plain) (From Petitta and Tallini, 2003). 1 - soil sediment, alluvial and talus deposit, conglomerate, calcareous breccia (Holocene - Middle Pleistocene); 2 - carbonate unit (Meso-Cenozoic); 3 - potentiometric line; 4 - spring; 5 - well; 6 - monitored wells; 7 - monitored river site; 8 - river discharge decrease; 9 - streambed spring (Aterno River); 10 - hydrogeological section (a - alluvial deposit; b - talus deposit; c - conglomerate, calcareous breccia; d - clay and sand; e - limestone and marl; f - limestone and marl; g - normal fault with cataclasite)

2.4 Earthquake hydrology

2.4.1 Introduction

Detecting earthquake precursors is one of the most compelling challenges in Earth sciences. Groundwater changes induced by seismic cycle have been widely documented all over the world including pre- co- and post- seismic responses (Wakita et al., 1975; Muir-Wood and King, 1993; Wang and Manga, 2021). Many studies shed light on the variation of crustal fluids behaviour after the occurrence of seismic events (postseismic). However, in the last decades attempts to identify preseismic anomalies have been carried out too (Wakita et al., 1980; Igarashi et al., 1995; Ingebritsen and Manga, 2014). In particular, changes in spring and river discharge (Petitta et al., 2018), groundwater level (Hwang et al., 2020; Lan et al., 2021), geochemical content (Kim et al., 2020), isotope composition (Skelton et al., 2014; Onda et al., 2018; Hosono et al., 2020), dissolved and free gases (Sano et al., 2016) have been recognized. Most of the interpretations agree in attributing hydrogeochemical anomalies to groundwater mixing between different aquifers driven by crustal

dilation process, permeability changes, pore pressure variations and so on (Tsunogai and Wakita, 1995; Claesson et al., 2004; Doglioni et al., 2014; Skelton et al., 2014; Andr n et al., 2016). To deepen understanding the earthquake-groundwater interaction, in some cases the related geochemical models have been also developed (W steb y et al., 2014; Boschetti et al., 2019). Despite these scientific efforts, the knowledge about hydrogeochemical behaviour related to the seismic cycle need more observations to carry out a statistical analysis aimed at identifying a common denominator. In particular, the three main questions that are searching for answers are: When, Where and How the next earthquakes will occur. To achieve this objective, several study cases are necessary to build up appropriate geochemical models. This goal can be reached only through the increase of observations that can help to provide useful constraints on models (Wang and Manga, 2021). Towards this direction, since 2014, a multiparametric monitoring network has been developed in central Italy with the main aim of identifying preseismic signals in groundwater (Barberio et al., 2017; 2020; Boschetti et al., 2019; Barbieri et al., 2020; 2021; Franchini et al., 2020; Coppola et al., 2021).

2.4.2 Earthquake hydrology of Abruzzi region

The groundwater flow within the main aquifers of the Abruzzi region (i.e. carbonate aquifers), is the result of the interaction between the elements of the hydrogeological cycle (rainfall and snow precipitation, evapotranspiration, runoff, infiltration), the geological and geomorphological features (e.g. fracture network and the lithological and karst characteristics), and, last but not least, the anthropic activities. These elements can affect the recharge-discharge processes with effects of superimposition, so to render very difficult the estimation of the single contribution of each element to the final outflow (Duran et al., 2020). In any case, currently, the study of carbonate aquifer is based on conceptual model and/or physically founded model which are however still uncertain (Hartmann et al., 2014).

Recently, the Apennine carbonate aquifers have been analysed as concerns the hydrological modifications due to the main recent earthquakes events occurred in the Abruzzi region (April 6th, 2009 Mw 6.3 L'Aquila seismic event and the 2016 central Italy seismic sequence Mw 6.0 Amatrice earthquake and Mw 6.5 Vettore Mt. seismic event), with a common observation of the discharge increase of spring and streamflow and changes of water table (De Luca et al., 2018; Petitta et al., 2018; Mastroiillo et al., 2020).

Lately, Scorzini et al. (2023) evidenced that deep learning algorithms replicate the groundwater flow of the Gran Sasso carbonate aquifer during significant earthquakes (i.e. the 2009 L'Aquila earthquake and the 2016 central Italy seismic sequence).

Further, considering that fluid flow along fault zones is a key aspect for seismicity migration and heat and chemical transfer, Chiarabba et al. (2022) evidenced that time-repeated seismic tomography showed Vp and Vp/Vs changes during the 2009 L'Aquila seismic sequence. This evidence could display a post-failure fluid rising up from hypocentral zone to the shallow layers, with a volume of about 5-100 million of cubic meters at flow rates up to 100 m/day.

Moreover, due to the upwelling of deep crustal fluids and geogas, such as radon, in seismic areas, hydrochemical and groundwater monitoring is regarded as a pivotal approach to study seismic signals of rocks undergoing accelerated strain transient (Barberio et al., 2017 and reference therein).

In the Abruzzi region, the case study of hydrogeochemistry of Gran Sasso groundwater versus April 6, 2009 M 6.3 L'Aquila earthquake can be regarded paradigmatic due co-seismic and post-seismic changes observed in groundwater discharge and hydrogeochemistry induced by L'Aquila earthquake (Adinolfi Falcone et al., 2012) considering that the Paganica fault accountable for the earthquake and its epicenter are placed in the Gran Sasso aquifer.

Spot and monitoring measurements of spring discharge, water table level and the main physico-chemical parameters of spring waters (T, pH, electrical conductivity, major ions and radon) were carried out and

compared with available data collected since the 1990s with the goal to determine the effects of L’Aquila earthquake on groundwater at regional and local scale (figs. 2.7-2.11).

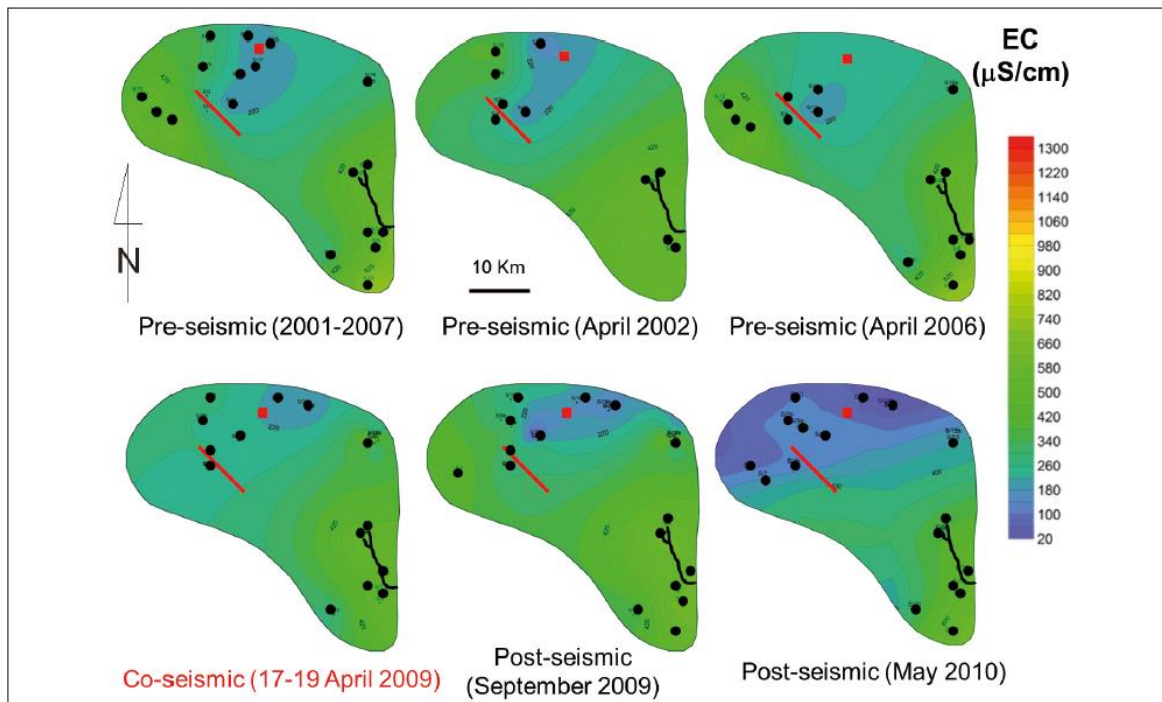


Figure 2.7: Electrical conductivity (EC) ($\mu\text{S/cm}$) isopleths of Gran Sasso aquifer, based on measured springs and drainages (black dots). The red line corresponds to the Paganica fault accountable for 2009 L’Aquila earthquake, red square to LNGS underground laboratories and black branch to Tirino River (Adinolfi Falcone et al., 2012)

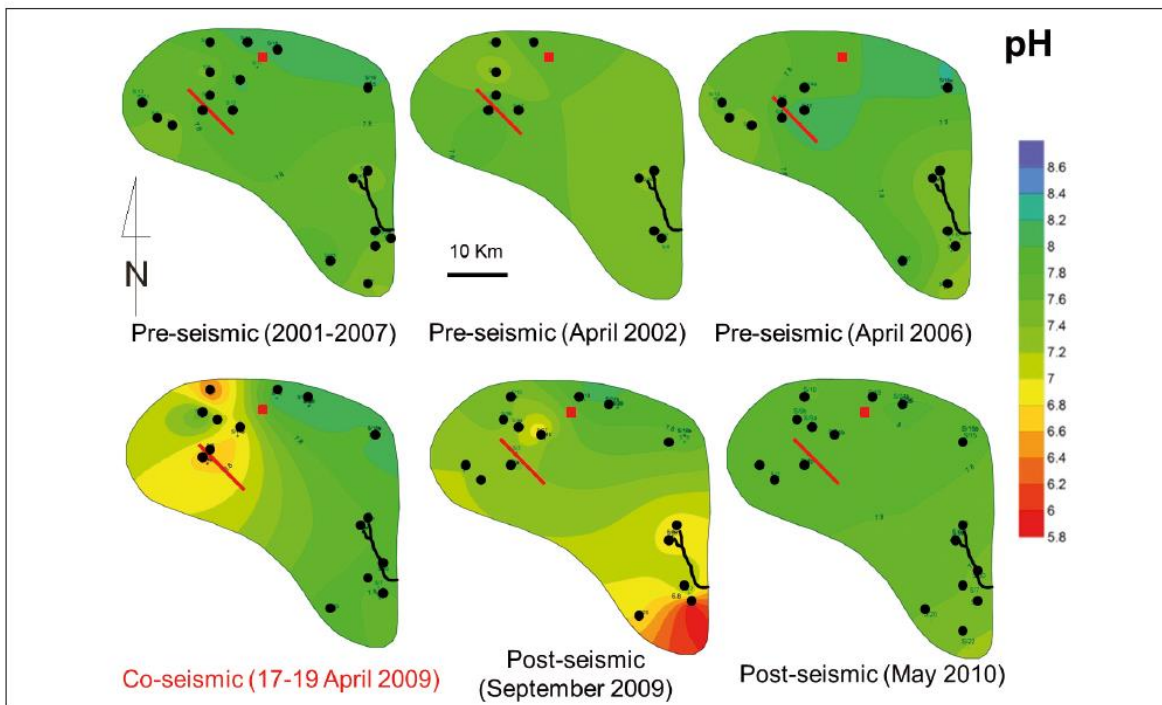


Figure 2.8: pH isopleths of Gran Sasso aquifer, based on measured springs and drainages (black dots). The red line corresponds to the Paganica fault accountable for 2009 L’Aquila earthquake, red square to LNGS underground laboratories and black branch to Tirino River (Adinolfi Falcone et al., 2012)

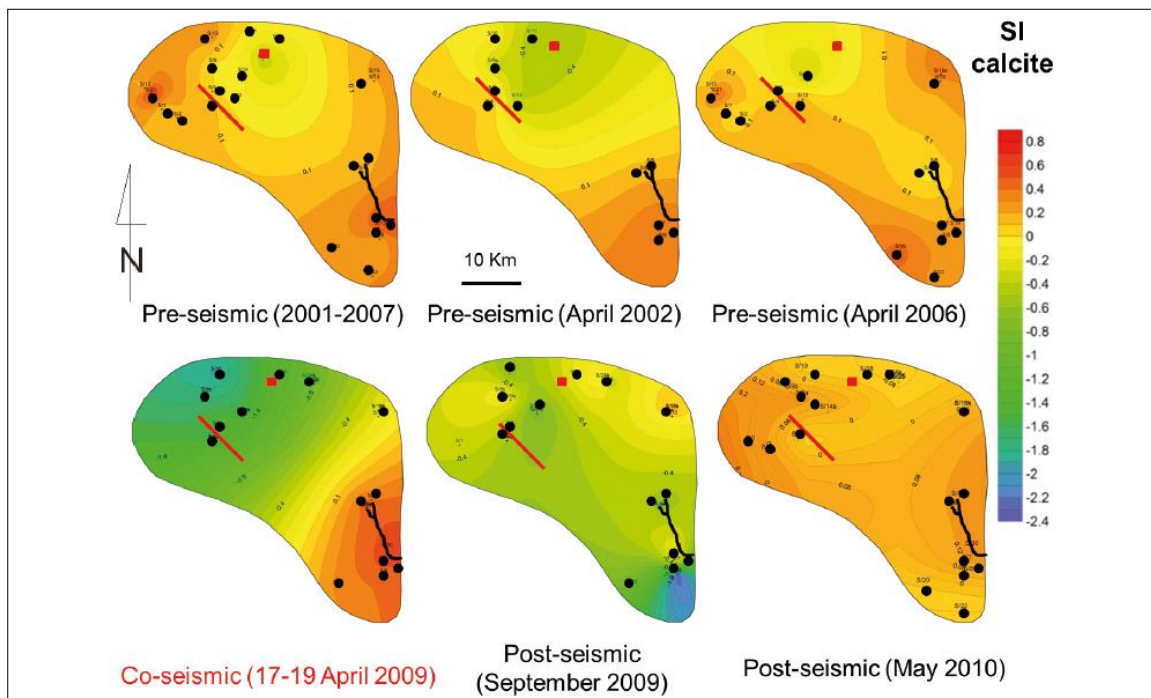


Figure 2.9: Calcite Saturation Index (SI) isopleths of Gran Sasso aquifer, based on measured springs and drainages (black dots). The red line corresponds to the Paganica fault accountable for 2009 L’Aquila earthquake, red square to LNGS underground laboratories and black branch to Tirino River (Adinolfi Falcone et al., 2012)

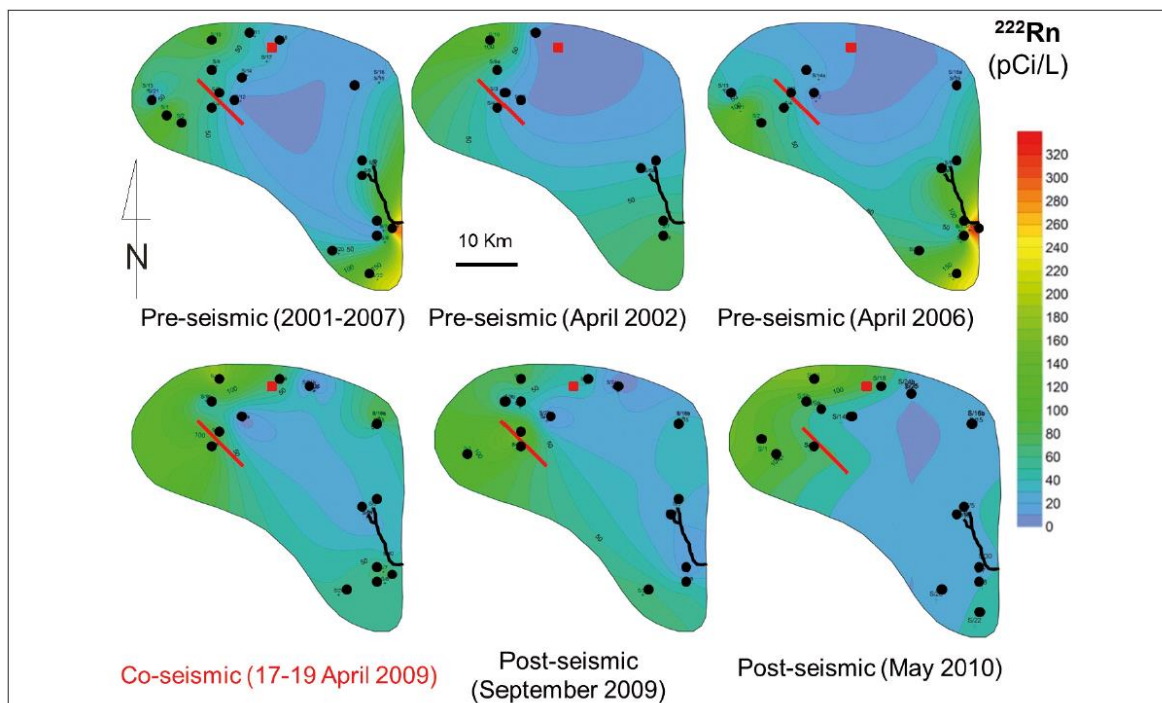


Figure 2.10: Radon content in groundwater (pCi/L - 1 pCi/L = 0.037 Bq/L) isopleths of Gran Sasso aquifer, based on measured springs and drainages (black dots). The red line corresponds to the Paganica fault accountable for 2009 L’Aquila earthquake, red square to LNGS underground laboratories and black branch to Tirino River (Adinolfi Falcone et al., 2012)

The outcomes of the hydrochemical spot sampling of the pre-seismic (2001-2007), post-seismic (April 2009) and after-seismic (July and September 2009, May 2010) periods, give the following insights (Adinolfi Falcone et al., 2012):

- i) post-seismic groundwater of Tempera spring group located along the Paganica active fault accountable for l'Aquila earthquake, was more mineralised and richer in radon than the pre-seismic one;
- ii) transient changes in pH and calcite saturation index involve the whole aquifer, moving from Tempera springs and spreading from the recharge to discharge areas, causing changes in groundwater hydrogeochemistry;
- iii) post-seismic gradual return to previous hydrochemical equilibrium.

The hydrochemical data acquired during L'Aquila earthquake are interesting within the goal of the artEmis project, and so Gran Sasso aquifer can be selected as a significant candidate area in which located the groundwater monitoring sites because it is crossed by many active faults and hosts remarkable groundwater resources.

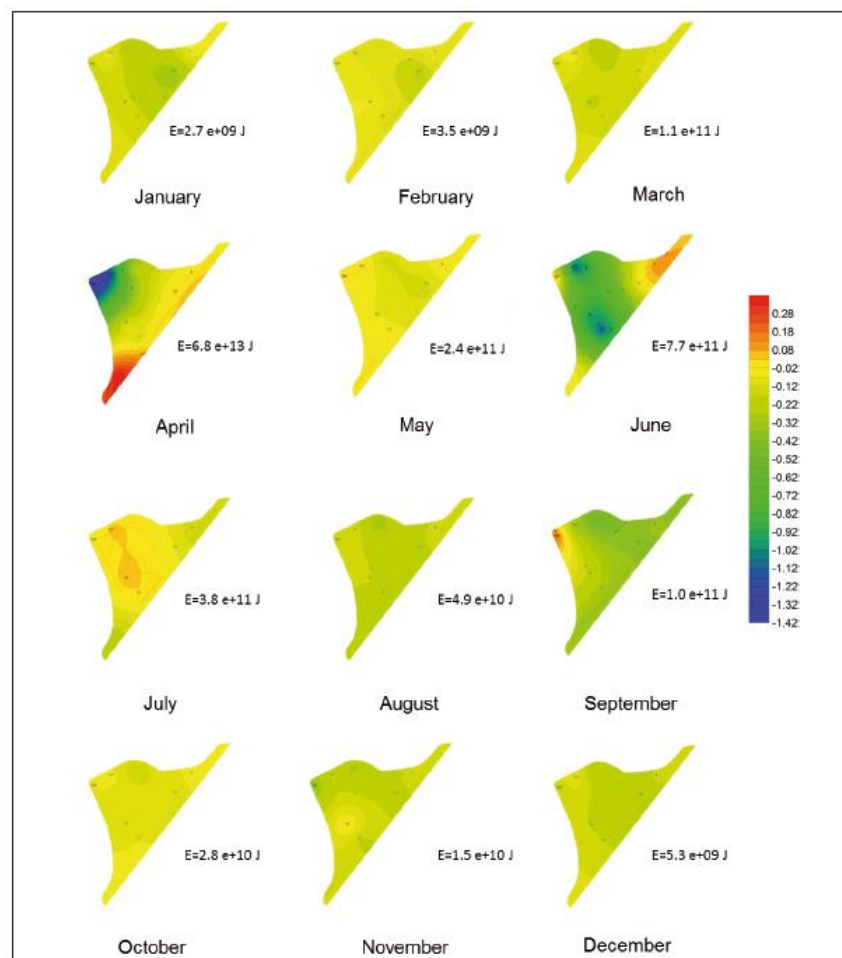


Figure 2.11: SI calcite monthly changes in the LNGS Gran Sasso underground lab during 2009 with monthly released seismic energy (E) in Joule. L'Aquila earthquake (M 6.3) occurred on April 6, 2009 (Adinolfi Falcone et al., 2012). LNGS are located about 20 km northeastward with respect to L'Aquila earthquake epicenter. Note the inverse correlation between the SI calcite values and the released seismic energy (e.g. April and June 2009)

2.5 References

- Adinolfi Falcone, R., Carucci, V., Falgiani, A., Manetta, M., Parisse, B., Petitta, M., Rusi, S., Spizzico, M., Tallini, M., 2012. Changes on groundwater flow and hydrochemistry of the Gran Sasso carbonate aquifer after 2009 L'Aquila earthquake. *Ital. J. Geosci.* 131 (3), 459–474. <https://doi.org/10.3301/IJG.2011.34>
- Adinolfi Falcone, R., Falgiani, A., Parisse, B., Petitta, M., Spizzico, M., Tallini, M., 2008. Chemical and isotopic ($d18O\%$, $d2H\%$, $d13C\%$, $222Rn$) multi-tracing for groundwater conceptual model of carbonate aquifer (Gran Sasso INFN underground laboratory— central Italy). *J Hydrol* 357, 368–388. [DOI:10.1016/j.jhydrol.2008.05.016](https://doi.org/10.1016/j.jhydrol.2008.05.016)
- Amoruso, A., Crescentini, L., Petitta, M., Rusi, S., Tallini, M., 2011. Impact of the 6 April 2009 L'Aquila earthquake on groundwater flow in the Gran Sasso carbonate aquifer, Central Italy. *Hydrol. Process.* 25 (11), 1754–1764. <https://doi.org/10.1002/hyp.7933>
- Andrén, M., Stockmann, G., Skelton, A., Sturkell, E., Mörth, C. M., Guðrúnardóttir, H. R., Keller, N.S., Odling, N., Dahrén, B., Broman, C., Balic-Zunic, T., Hjartarson, H., Siegmund, H., Freund, F., Kockum, I., 2016. Coupling between mineral reactions, chemical changes in groundwater, and earthquakes in Iceland. *J. Geophys. Res. Solid Earth* 121(4), 2315–2337.
- Barberio, M. D., Gori, F., Barbieri, M., Billi, A., Caracausi, A., De Luca, G., Franchini, S., Petitta, M., Doglioni, C., 2020. New observations in Central Italy of groundwater responses to the worldwide seismicity. *Sci. Rep.* 10, 1–10.
- Barberio, M.D., Barbieri, M., Billi, A., Doglioni, C., Petitta, M., 2017. Hydrogeochemical changes before and during the 2016 Amatrice-Norcia seismic sequence (central Italy). *Sci. Rep.* 7 (1), 1–12. <https://doi.org/10.1038/s41598-017-11990-8>
- Barberio, M.D., Gori, F., Barbieri, M., Boschetti, T., Caracausi, A., Cardello, G.L., Petitta, M., 2021. Understanding the Origin and Mixing of Deep Fluids in Shallow Aquifers and Possible Implications for Crustal Deformation Studies: San Vittorino Plain, Central Apennines. *Appl. Sci.* 11(4), 1353.
- Barbieri, M., Boschetti, T., Barberio, M.D., Billi, A., Franchini, S., Iacumin, P., Selmo, E., Petitta, M., 2020. Tracing deep fluid source contribution to groundwater in an active seismic area (central Italy): A combined geothermometric and isotopic ($\delta13C$) perspective. *J. Hydrol.* 582, 124495. <https://doi.org/10.1016/j.jhydrol.2019.124495>
- Barbieri, M., Boschetti, T., Petitta, M., Tallini, M., 2005. Stable isotopes ($2H$, $18O$ and $87Sr/86Sr$) and hydrochemistry monitoring for groundwater hydrodynamics analysis in a karst aquifer (Gran Sasso, Central Italy). *Appl Geochem* 20, 2063–2081. <https://doi.org/10.1016/j.apgeochem.2005.07.008>
- Barbieri, M., Franchini, S., Barberio, M. D., Billi, A., Boschetti, T., Giansante, L., Gori, F., Jónsson, S., Petitta, M., Skelton, A., Stockmann, G., 2021. Changes in groundwater trace element concentrations before seismic and volcanic activities in Iceland during 2010–2018. *Sci. Total Environ.* 148635.
- Boni, C., 2000. Karst aquifers of the Central Apennines. *Hydrogéologie* 4, 49-62.
- Boni, C., Bono, P., Capelli, G., 1986. Schema idrogeologico dell'Italia Centrale [Hydrogeological scheme of Central Italy]. *Mem. Soc. Geol. It.* 35, 991-1012, with hydrogeological maps at 1:500,000 scale.
- Boschetti, T., Barbieri, M., Barberio, M.D., Billi, A., Franchini, S., Petitta, M., 2019. CO₂ Inflow and Elements Desorption Prior to a Seismic Sequence, Amatrice-Norcia 2016, Italy. *Geochem. Geophys. Geosyst.* 20(5), 2303–2317. <https://doi.org/10.1029/2018GC008117>
- Celico, P., 1983. Idrogeologia dei massicci carbonatici, delle piane quaternarie e delle aree vulcaniche dell'Italia centro-meridionale: Progetti speciali per gli schemi idrici nel Mezzogiorno [Hydrogeology of

carbonate massifs, Quaternary plains and volcanic areas of Central-Southern Italy: Special projects for water schemes in Southern Italy]. *Quad. Cassa Mezzog.*, 4/2, 1-225.

[extension://efaidnbmnnnibpcajpcglclefindmkaj/https://aset.acs.beniculturali.it/dm_0/00/high/biblio/pdf/Quaderno-4_2.pdf](https://efaidnbmnnnibpcajpcglclefindmkaj/https://aset.acs.beniculturali.it/dm_0/00/high/biblio/pdf/Quaderno-4_2.pdf) (accessed 4.21.23).

Chiarabba, C., De Gori, P., Valoroso, L., Petitta, M., Carminati, E., 2022. Large extensional earthquakes push-up terrific amount of fluids. *Sci Rep* 12, 14597. <https://doi.org/10.1038/s41598-022-18688-6>

Claesson, L., Skelton, A., Graham, C., Dietl, C., Mörth, M., Torssander, P., Kockum, I., 2004. Hydrogeochemical changes before and after a major earthquake. *Geology* 32, 641. <https://doi.org/10.1130/G20542.1>

Coppola, M., Correale, A., Barberio, M. D., Billi, A., Cavallo, A., Fondriest, M., Nazzari, M., Paonita, A., Romano, C., Stagno, V., Viti, C., Vona, A., 2021. Meso-to nano-scale evidence of fluid-assisted co-seismic slip along the normal Mt. Morrone Fault, Italy: Implications for earthquake hydrogeochemical precursors. *Earth Planet. Sci. Lett.* 568, 117010.

De Luca, G., Di Carlo, G., Tallini, M., 2018. A record of changes in the Gran Sasso groundwater before, during and after the 2016 Amatrice earthquake, central Italy. *Sci. Rep.* 8 (1), 1–16. <https://doi.org/10.1038/s41598-018-34444-1>

Doglioni, C., Barba, S., Carminati, E., Riguzzi, F., 2014. Fault on–off versus coseismic fluids reaction. *Geosci. Front.* 5, 767–780. <https://doi.org/10.1016/j.gsf.2013.08.004>

Duran, L., Massei, N., Lecoq, N., Fournier, M., Labat, D., 2020. Analyzing multi-scale hydrodynamic processes in karst with a coupled conceptual modeling and signal decomposition approach. *J. Hydrol.* 583, 124625. <https://doi.org/10.1016/j.jhydrol.2020.124625>

Franchini, S., Agostini, S., Barberio, M.D., Barbieri, M., Billi, A., Boschetti, T., Pennisi, M., Petitta, M., 2020. HydroQuakes, central Apennines, Italy: Towards a hydrogeochemical monitoring network for seismic precursors and the hydro-seismo-sensitivity of boron. *J. Hydrol.* 125754. <https://doi.org/10.1016/j.jhydrol.2020.125754>

Hartmann, A., Goldscheider, N., Wagener, T., Lange, J., Weiler, M., 2014. Karst water resources in a changing world: Review of hydrological modeling approaches. *Rev. Geophys.* 52 (3), 218–242. <https://doi.org/10.1002/2013RG000443>.

Hosono, T., Yamada, C., Manga, M., Wang, C.-Y., Tanimizu, M., 2020. Stable isotopes show that earthquakes enhance permeability and release water from mountains. *Nat. Commun.* 11, 2776. <https://doi.org/10.1038/s41467-020-16604-y>

Hwang, H. S., Hamm, S. Y., Cheong, J. Y., Lee, S. H., Ha, K., Lee, C., Woo, N.C., Yun, S.M., Kim, K. H., 2020. Effective time-and frequency-domain techniques for interpreting seismic precursors in groundwater level fluctuations on Jeju Island, Korea. *Sci. Rep.* 10(1), 1–14.

Igarashi, G., Saeki, S., Takahata, N., Sumikawa, K., Tasaka, S., Sasaki, Y., Takahashi, M., Sano, Y., 1995. Ground-Water Radon Anomaly Before the Kobe Earthquake in Japan. *Science* 269, 60–61. <https://doi.org/10.1126/science.269.5220.60>

Ingebritsen, S. E., Manga, M., 2014. Hydrogeochemical precursors. *Nat. Geosci.* 7(10), 697–698.

Kim, J., Lee, J., Petitta, M., Kim, H., Kaown, D., Park, I. W., Lee, S., Lee, K. K., 2019. Groundwater system responses to the 2016 ML 5.8 Gyeongju earthquake, South Korea. *J. Hydrol.* 576, 150–163.

Lan, S., Gu, H., Yu-Liu, 2021. Changes in groundwater level and tidal response caused by the Wenchuan earthquake, China. *Hydrogeol. J.* <https://doi.org/10.1007/s10040-021-02302-6>

- Manga, M. Wang, C.Y., 2015. Earthquake Hydrology. In: Schubert, G. (Eds.), *Treatise on Geophysics*, 2nd Edition, Vol 4. Oxford: Elsevier, 305–328. [doi: 10.1016/B978-0-444-53802-4.00082-8](https://doi.org/10.1016/B978-0-444-53802-4.00082-8)
- Mastrorillo, L., Saroli, M., Viaroli, S., Banzato, F., Valigi, D., Petitta, M., 2020. Sustained post-seismic effects on groundwater flow in fractured carbonate aquifers in Central Italy. *Hydrol. Process.* 34 (5), 1167–1181. <https://doi.org/10.1002/hyp.13662>
- Mohr, C.H., Manga, M., Wang, C.Y., Korup, O., 2017. Regional changes in streamflow after a megathrust earthquake. *Earth Planet. Sci. Lett.* 458, 418–428. <https://doi.org/10.1016/j.epsl.2016.11.013>
- Muir-Wood, R., King, G.C.P., 1993. Hydrological signatures of earthquake strain. *J. Geophys. Res.* 98, 22035–22068. <https://doi.org/10.1029/93JB02219>
- Onda, S., Sano, Y., Takahata, N., Kagoshima, T., Miyajima, T., Shibata, T., Pinti, D.L., Lan, T., Kim, N.K., Kusakabe, M., Nishio, Y., 2018. Groundwater oxygen isotope anomaly before the M6. 6 Tottori earthquake in Southwest Japan. *Sci. Rep.* 8 (1), 1–7. <https://doi.org/10.1038/s41598-018-23303-8>
- Petitta, M., Mastrorillo, L., Preziosi, E., Banzato, F., Barberio, M.D., Billi, A., Cambi, C., De Luca, G., Di Carlo, G., Di Curzio, D., Di Salvo, C., Nanni, T., Palpacelli, S., Rusi, S., Saroli, M., Tallini, M., Tazioli, A., Valigi, D., Vivalda, P., Doglioni, C., 2018. Watertable and discharge changes associated with the 2016–2017 seismic sequence in central Italy: hydrogeological data and a conceptual model for fractured carbonate aquifers. *Hydrogeology Journal*, 26 (4), 1009–1026. [DOI: 10.1007/s10040-017-1717-7](https://doi.org/10.1007/s10040-017-1717-7)
- Petitta, M., Rusi, S., Salvati, R., 2003. Risorse idriche, in: Crescenti, U., Miccadei, E., Praturlon, A. (Eds.), *Guide Geologiche Regionali – Abruzzo [Regional Geological Guides – Abruzzi]*, edited by Società Geologica Italiana, BE-MA Editrice, Milano.
- Petitta, M., Tallini, M., 2003. Groundwater resources and human impacts in a Quaternary intramontane basin (L'Aquila Plain, Central Italy). *Water International*, 28 (1), 57–69. [doi: 10.1080/02508060308691665](https://doi.org/10.1080/02508060308691665)
- Petitta, M., Tallini, M., 2002. Idrodinamica sotterranea del massiccio del Gran Sasso (Abruzzo): indagini idrologiche, idrogeologiche e idrochimiche (1994–2001) [Underground hydrodynamics of the Gran Sasso massif (Abruzzo): hydrological, hydrogeological and hydrochemical investigations (1994–2001)]. *Boll. Soc. Geol. D'It.* 121, 343–363
- Sano, Y., Takahata, N., Kagoshima, T., Shibata, T., Onoue, T., Zhao, D., 2016. Groundwater helium anomaly reflects strain change during the 2016 Kumamoto earthquake in Southwest Japan. *Sci. Rep.* 6, 37939. <https://doi.org/10.1038/srep37939>
- Scorzini, A. R., Di Bacco, M., De Luca, G., Tallini, M., 2023. Deep learning for earthquake hydrology? Insights from the karst Gran Sasso aquifer in central Italy. *Journal of Hydrology*, 617, 129002. <https://doi.org/10.1016/j.jhydrol.2022.129002>
- Scozzafava, M., Tallini, M., 2001. Net infiltration in the Gran Sasso Massif (Central Italy): thornthwaite water budget using the CN method (Soil Conservation Service). *Hydrogeology Journal* 9, 461–475. <https://doi.org/10.1007/s100400100151>
- Skelton, A., Andrén, M., Kristmannsdóttir, H., Stockmann, G., Mörth, C.-M., Sveinbjörnsdóttir, Á., Jónsson, S., Sturkell, E., Guðrúnardóttir, H.R., Hjartarson, H., Siegmund, H., Kockum, I., 2014. Changes in groundwater chemistry before two consecutive earthquakes in Iceland. *Nat. Geosci.* 7, 752–756. <https://doi.org/10.1038/ngeo2250>
- Tsunogai, U., Wakita, H., 1995. Precursory chemical changes in ground water: Kobe earthquake, Japan. *Science*, 269(5220), 61–63.

Wakita, H., 1975. Water Wells as Possible Indicators of Tectonic Strain. *Science* 189, 553–555. <https://doi.org/10.1126/science.189.4202.553>

Wakita, H., Nakamura, Y., Notsu, K., Noguchi, M., Asada, T., 1980. Radon anomaly: a possible precursor of the 1978 Izu-Oshima-kinkai earthquake. *Science* 207(4433), 882–883.

Wang, C. Y., Manga, M., 2021. Earthquakes influenced by water. In *Water and Earthquakes* (pp. 61-82). Cham: Springer International Publishing.

Wästeby, N., Skelton, A., Tollefsen, E., Andrén, M., Stockmann, G., Claesson Liljedahl, L., Sturkell, E., Mörth, M., 2014. Hydrochemical monitoring, petrological observation, and geochemical modeling of fault healing after an earthquake: Fault healing after an earthquake. *J. Geophys. Res. Solid Earth* 119, 5727–5740. <https://doi.org/10.1002/2013JB010715>

3 Hydrogeology of the Ionian Islands and the Gulf of Corinth (Greece)

3.1 Hydrogeology of central Ionian islands

3.1.1 Hydrogeology of Lefkada island

Lefkada Island is mainly covered by the permeable carbonate formations of Ionian and Paxos Zones, resulting in a hydrogeological setting which is characterized by groundwater karstic systems without significant surface run off (Figure 3.1). Lefkada's groundwater system covers an area equal to 92 km². The system is composed by the alluvial basins (formations with light and dark yellow colors in Figure 3.1) that are developed in northern part (town of Lefkada), in the southern part (Vasiliki village) and in the eastern part (Nydrri village) and the permeable karstic aquifers (formations with light and dark green colors in Figure 3.1) which surround the modern deposits.

The permeability, k , of the groundwater system is ranging from 10^{-3} to 10^{-7} m/sec. The water system in its northern part has a direct connection with the lagoons of Avlemonas and Paleo, located north-northeast of Lefkada's town (Figure 3. 2). The groundwater aquifers are recharged by rainfall, direct penetration and in a small percentage through lateral transfers from the karstic formations. It is estimated that the average annual supply amounts to $10 \times 10^6 \text{ m}^3$ of water (Special Secretariat for Water, 2014).

The most significant water sources of Lefkada are mainly consisting of spring and fountains in the middle and southern part of the island (light blue circles in Figure 3.2). Additionally, the existence of the canyon and waterfall near Vafkeri village at the middle part of the island is also observed (dark blue hexagon in map of Figure 3.2). Starting from the northern part of the island, near to the Lefkada town, the spring *Big Fountain* is located. The area was named after the spring and it is located in the municipal department of Kalligoni, in Lefkada's Municipality. The water of the spring feed the town of Lefkada and the settlements of the wide area. The *Vafkeri* spring is located in the middle part of the island, in the area west of the homonymous municipal department. The spring is extended under the planes with 8 vents from where the abundant water of the spring flows. The area where water of the spring flows, belongs to the formations of Ionian zone, while its feed has a relation to the incumbent formations of Paxoi zone (Figure 3.1). The spring supply is $50 \text{ m}^3/\text{hour}$ during winter period and its water is used for the watering of the settlement and for irrigation purposes. Springs *Sfaelia* and *Koutreli* are located 1.5 km southeast of Vafkeri village and their total water supply is equal to $320 \text{ m}^3/\text{day}$ during summer and they are mainly used for irrigation purposes. In the same area, the *Dimossari* waterfall and canyon is located. The water course of the waterfall is surrounded by savage slopes with vivid aptitudes and impervious vegetation such as hollies, and oleasters. Small lakes are formed among rocky water courses and vertical slopes along the river to 500 meters before its extrusion to the sea. The height of the waterfall reaches to 12 meters, while the length of the cavity reaches 8 meters.

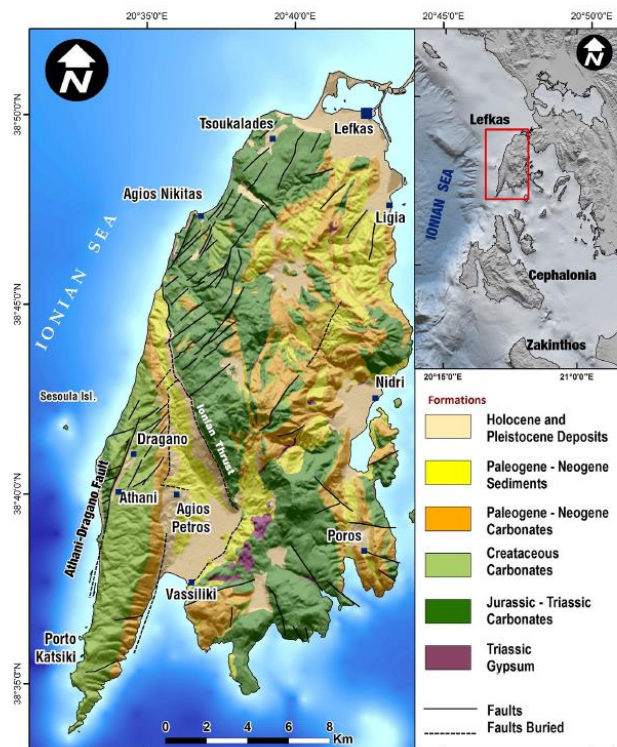


Figure 3.1: Geological formations map of Lefkada island in which the alluvial and the carbonate formations are denoted with the yellow (light and dark) and green (light and dark) colors, along with its tectonic setting (after Cushing, 1985, Rondoyanni et al., 2007 and Papathanasiou et al., 2017)

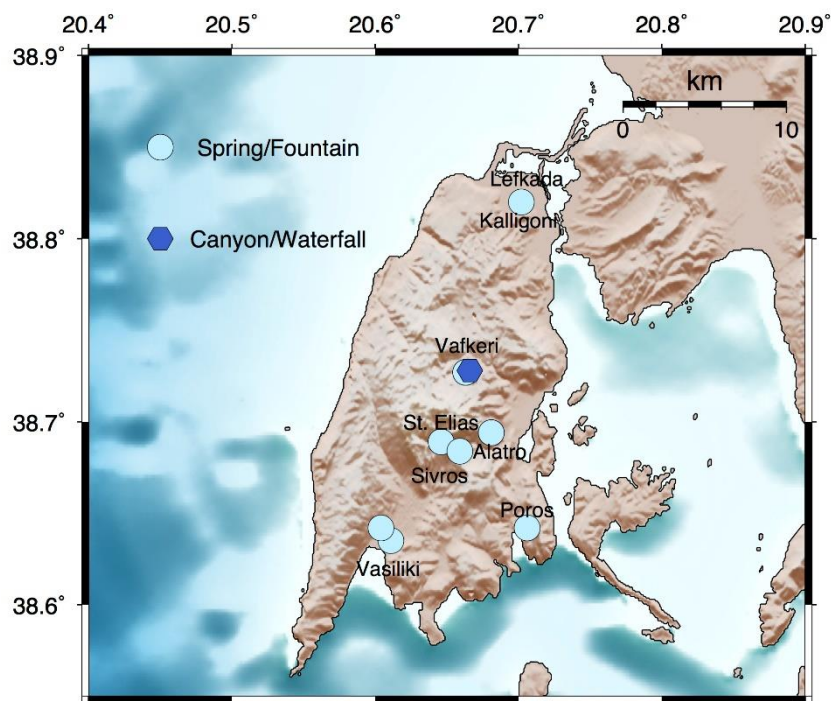


Figure 3.2: Morphological map of Lefkada island with its main springs/fountains and canyons/waterfalls denoted by the light blue circles and the dark blue hexagon, respectively

In the middle part of the island a cluster of several springs is also extended (Figure 3.2). In detail, the springs *Vrissouli*, *Manasi* and *Saint Ilias* are located north of the Sivros village. *Vrissouli* and *Manasi* springs are located in the foot of Stavrota mountain and belong to the spring system that appears along the Ionian zone front and along Paxoi zone. The water supply of the springs is 110 m³/day during summer and it is mainly used for irrigation purposes. *Saint Elias* spring is located in the mansion of the homonymous settlement. The water supply of the spring is varying from 30 to 80 m³/hour and is used for the irrigation of Sivros settlement and for other irrigation purposes. Moving to the east, the *Vrissi* spring is located north of Alatros settlement (Figure 3.2). The spring is at the point where limestones and flysches are mixed, right in the formation of Ionian zone. The supply of the spring is 20-25 m³/hour, while in September the water flow notably decreases. Spring water is mainly used for the irrigation of Alastro's settlement.

In the southeastern part of Lefkada island, the spring *Megalos Lompos* in Poros settlement is located (Figure 3.2). The spring is northwest of Poros settlement in altitude of 40 m above the sea level, upon the formations of Paxoi zone. It flows from Cretaceous limestones. Moving to the southwest part of Lefkada, the cluster of Vassiliki's springs is located. The springs are near the sea and adjoin it to the west of the settlement. The water of the spring flows to the Holocene formation. Water of the cluster of Vassiliki's springs remain unexploited as it concerns the irrigation of the settlements in the broader area. The only operation of spring water is the feed of the watermill which is located in the area of the springs and it works until today. Table 3.1 summarizes all the available information about the water sources of Lefkada island, as reported previously. In the central and southern part of Lefkada island, there is a big number of traditional wells which are functional and are used for irrigation purposes. The depths from the earth's surface to their bottom range from 7 to 12 meters. Most of them have diameters up to four meters. There is a seasonal fluctuation of the water surface about 1-3 meters depending on the amount of the precipitation each year. In the northern part of Lefkada, rainfall water collected in cisterns, was used in the past.

3.1.2 Hydrogeology of Kefalonia island

The Kefalonia hydrogeological conditions are very complex. Different karstic systems create a very interesting hydrodynamic regime, with high-capacity aquifers, spring discharges, and water outflows in the sea around it. The Island is mainly covered by carbonate formations, which are permeable. Because of the extended development of permeable formations, there is not significant surface run off, the total volume of rainfall infiltrates and recharges the karstic aquifers. The karstic systems of the Island are very complex because of the intense tectonism (Karymbalis et al., 2013).

The main mountain mass of Kefalonia Island is Aenos (1630 m a.s.l.) (Figure 3.3) occupying the central part of the island, oriented in a NW–SE direction. The principal water divide has the same direction with a well-developed drainage pattern on the eastern part of the main island where the two largest fifth-order (according to Strahler's classification system) networks exist. The main channel flow directions of these networks are to the NE (Sami Bay) and the SW (Poros), with the development of the main streams channels controlled by lithological contacts, faults and upthrusts. The coastal zone of the southern part of the main island consists of relatively steep slopes with relatively short streams of first and second order. The area bounding the eastern side of Argostoli Gulf, is characterized by very steep limestone cliffs (with slopes between 39 and 78%) due to the neotectonic origin of the Gulf (Gaki-Papanastasiou et al., 2011), with a small parallel not well-developed drainage network.

Source Number	Source Name	Location (Latitude/Longitude)	Details
1	<i>Avlemonas & Paleo Lagoons</i>	38.841/20.700	<ul style="list-style-type: none"> • Aver. Depth: 0.8 m • Max. Depth: 1.5 m
2	Spring <i>Big Fountain</i> in Kalligoni village	38.820/20.702	<ul style="list-style-type: none"> • feed Lefkada town • Supply: 700 m³/day • The spring is probably fed by limestones
3	<i>Dimossari</i> canyon & waterfall	38.728/20.666	<ul style="list-style-type: none"> • Height: 12 m • Cavity length: 8 m • Pool of 3 m depth
4	<i>Vefkeri</i> spring in Vefkeri village	38.727/20.663	<ul style="list-style-type: none"> • Spring with 8 vents • The area belongs to the formations of Ionian zone • Supply: 50 m³/hour (during winter)
5	<i>Sfaelia & Koutreli</i> springs of Vafkeri village	38.727/20.663	<ul style="list-style-type: none"> • 1500 m SE of Vafkeri) • Supply: 320 m³/day (during July) • The area belongs to the formations of Ionian zone (Eocene Limestones)
6	<i>Vryssouli & Manassi</i> springs	38.694/20.681	<ul style="list-style-type: none"> • The springs are located in the foot of Stavrota's mountain (Ionian & Paxoi Zones) • Supply: 110 m³/day (during summer)
7	<i>Saint Elias</i> springs	38.689/20.646	<ul style="list-style-type: none"> • Supply: 30 – 80 m³/hour
8	<i>Vrissi</i> spring in Alatro village	38.684/20.659	<ul style="list-style-type: none"> • Supply: 20-25 m³/hour, while in September the water flow notably decreases • Ionian Zone Formations
9	<i>Megalos Lompos</i> spring in Poros village	38.642/20.706	<ul style="list-style-type: none"> • It flows from Cretaceous limestones (Paxoi Zone)
10	Cluster of Vassiliki Springs	38.628/20.609	<ul style="list-style-type: none"> • The springs are near the sea with which they adjoin with the settlement in west. • The water of the spring flows from Holocene geological formations

Table 3.1: Summary of the location and the available information of the main water resources of Lefkada island

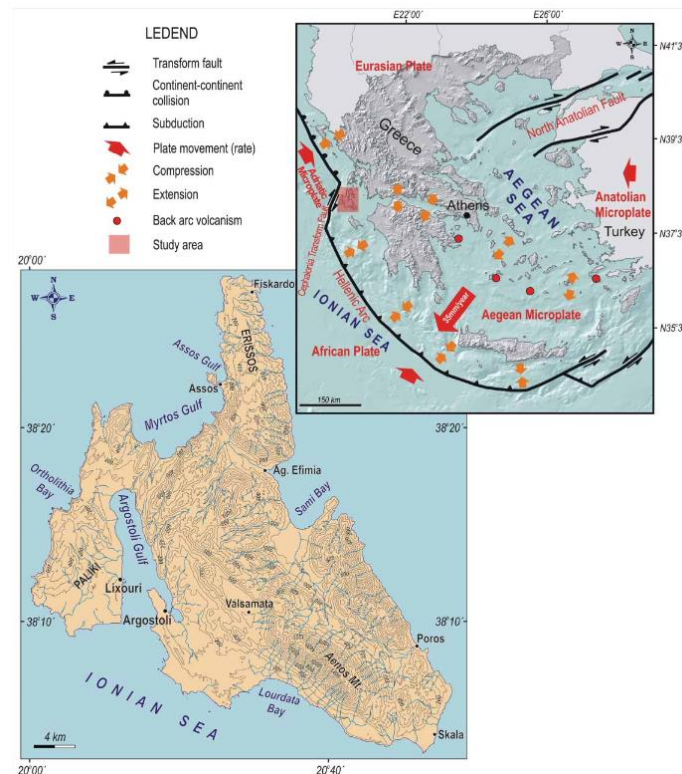


Figure 3.3: Topographic map of Kefalonia Island and location map depicting the geodynamic setting of the broader Aegean area (geodynamic setting map is based on Gaki-Papanastasiou, et al., 2011)

The Erissos Peninsula, the central part of which is an extensive, partially karstified, planation surface, is drained by short streams discharging directly into the sea. The eastern ones are more heavily incised probably due to higher tectonic uplift rates since the east almost straight cliffed shoreline of the peninsula is affected by a NNW–SSE trending coastal fault. The northeastern part of the Paliki peninsula is drained by three major drainage networks with the upper reaches flowing in a NNW–SSE direction and then turning to the east discharging into Argostoli Gulf. The uppermost parts of these drainage networks are the oldest as they have evolved on limestones of Eocene–Oligocene and Miocene age while their lowermost parts passing through the Pliocene formations are much younger (Gaki-Papanastasiou et al., 2010). These drainage networks were tributaries of a much larger drainage pattern which was active during the last glacial period up until early Holocene. The main channel of this drainage network had an almost N–S direction flowing along the eastern side of the present Argostoli Gulf which was a valley during the early Holocene (Gaki-Papanastasiou et al., 2011). The bathymetry of the gulf reveals that it is a shallow submarine valley with a maximum depth of about 25 m east of cape Ag. Georgios. Its western submarine slopes are less steep than the eastern ones probably due to structural reasons since the strata on the western Paliki peninsula are dipping toward the gulf as well as due to the deposition of sediments supplied by the drainage networks of the Paliki peninsula. At the southern part of the Paliki peninsula there are two drainage networks. Their upper parts have developed on limestone formations having a low drainage density while their more extensive lower parts drain Pliocene formations.

Six different karstic systems are developed in the Island. The karstic system of mountain Ainos (Ionian zone) is discharged by three coastal springs. These karstic systems have significant outflows to the sea. According to Koumantakis (1989), the most significant springs in the Island are: a) Springs of Agios Ioannis (200 m³/h) b) Papadatos springs (300 m³/h) in Koutavos, c) Springs of Avythos (100 m³/h), d) In the Sami moorage, the saline springs of Karavomylos and Agia Eufimia. All these springs are the surface discharge points from the

respectively karstic systems, but there are also many submarine springs with significant outflows to the sea. The karstic system of mountain Atros is discharged surficially by Avythos springs. The karstic system of Kalo Oros, at the north part of Kefalonia is exploited by drills and it is in hydraulic connection with the sea. Outflows also come from the karstic system of Paliki, at the area of Atheras. In Lixouri it is developed a semi-aquifer system in the alluvial deposits. In Argostoli there is a granular water system, where confined and unconfined aquifers are developed. The isohyet map of Kefalonia (Figure 3.4) shows the distribution of the mean annual precipitation (Katsafados et al., 2012), which ranges from 820 mm at the southern part of the island to more than 900 mm at its eastern part. According to 27 year records of the meteorological station located in Argostoli, precipitation is unevenly distributed during the year, with most falling during winter and the transient periods. The wettest months of the year are October, November, December, and January. All surface and ground water in the study area is the result of precipitation. Changes in climatic conditions such as precipitation and temperature can cause large and rapid changes in stream flow and more gradual changes in ground water flow. The streams of the island are seasonal flow and there are no discharge gauges.

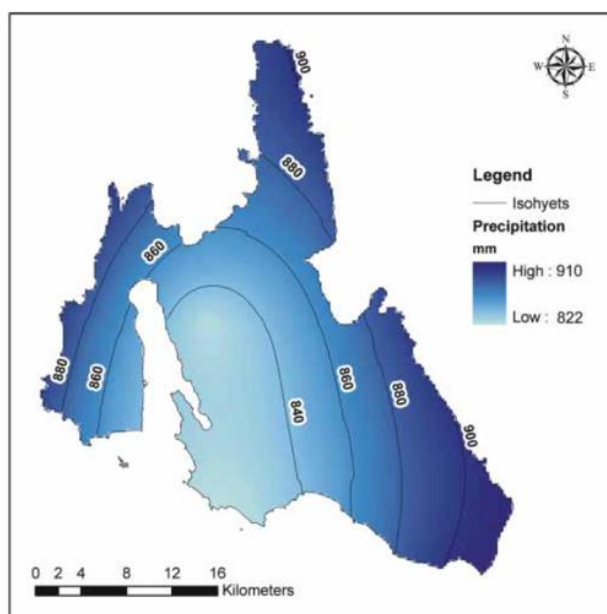


Figure 3.4: The isohyet map of Cephalonia using data from 1980 to 2001 (after Katsafados et al., 2012)

Chemical analysis of rainwater and mixed or ground water showed that the PH values range from 7.63 to 8.80 with a mean value of 8.35, indicated that in the studied area the rain is not acid. Rainwater has low-medium values for conductivity (medium conductivity $103 \mu\text{S cm}^{-1}$) and low-medium level of ions of marine origin (median Na^+ :6 ppm, Cl^- :7 ppm). Rainwater contains the elements Ca and Mg in relatively adequate concentrations. The highest value of hardness measured in rainwater was $74 \text{ mg l}^{-1} \text{ CaCO}_3$ and the median value was $40 \text{ mg l}^{-1} \text{ CaCO}_3$. Fluoride is not detected in rainwater while metals, either essential or toxic, are present in traces (Sazakli et al., 2007). In general, conductivity and most of the ions show lower values in rainwater than in mixed or ground water. Manganese and Cadmium are present in lower levels in rainwater than in other water, while mean PH was higher in rainwater (Sazakli et al., 2007). There is a seasonal variation for some main ions and consequently for conductivity, with higher values being detected in winter.

The water quality varies; the phenomenon of sea intrusion takes place in the coastal areas, because most of the karstic systems are open to the sea, or due to overexploitation of the aquifers. High salinity has measured in many samplings. The geochemical “pollution” is also presented in many cases because limestones are

soluble, so the chemical reaction of ion exchange is performed. The exploitation of the water resources is done by drillings wells and springs. According to IGME (2010) 97 drills, 30 wells and 18 springs were recorded, but the real number of the subtraction works are bigger than them (Figure 3.5). Stefouli et al. (2013) applied complementary techniques to localise coastal ground water discharge in the widespread carbonate coastal aquifer of Cephalonia Island. Large coastal discharges have been observed using remote sensing techniques and this provides important information concerning different parameters of interest to a hydrological project. The locations of water outflows seem to be associated with tectonic discontinuities, which are used as conduits for the subsurface water flow.

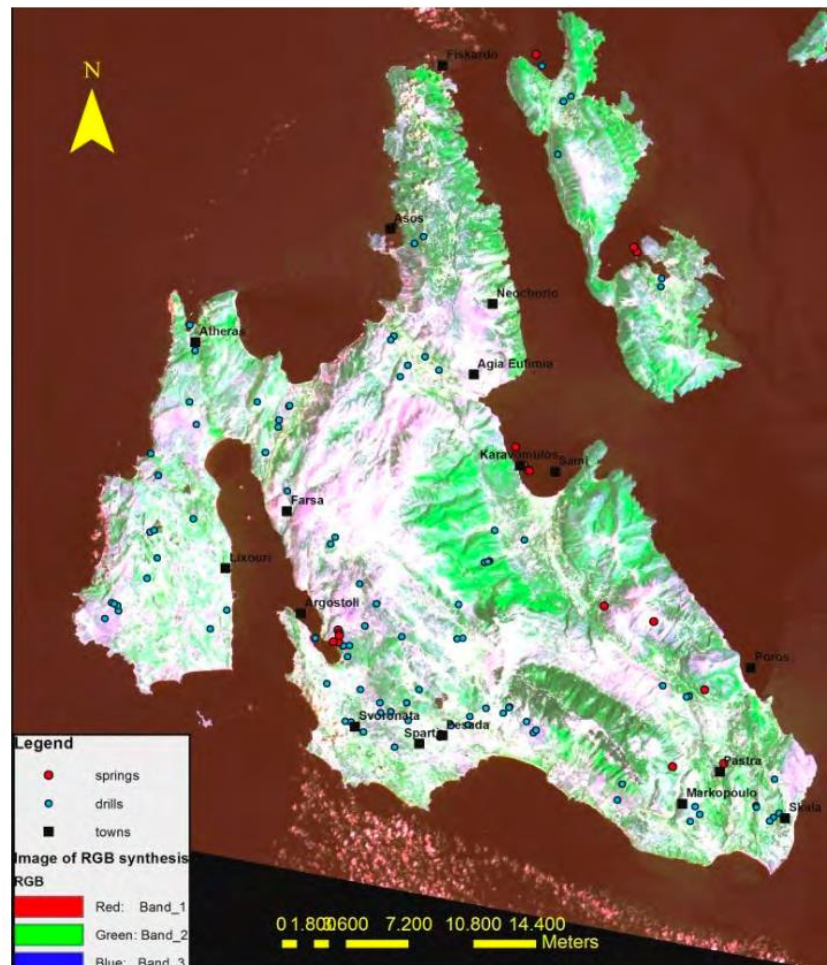


Figure 3.5: Satellite image of Cephalonia with the water point subtractions. (Stefouli et al., 2013)

3.2 Hydrogeology of Gulf of Corinth

The area of Gulf of Corinth has a complex geological structure, composing by formations belonging to Pelagonian, Parnassos, Pindos and Gavrovo – Tripolitsa zones from its Easternmost to its Southernmost margins, along with a large amount of Quaternary and Plio-Pleistocene sediments (Figure 3.6). In detail, the geological formations that can be identified are:

- Quaternary deposits consisting of alternations of sands and fine coarse or mixed facies. The thickness of the plain's deposits varies from 30 m to 70 m, whilst along the fluvio-torrential deposits of the rivers it exceeds 100 m. As a result of their origin the deposits are characterized by high degree of heterogeneity and anisotropy.

- Plio-Pleistocene deposits. They form the semi-mountainous region covering a large area and they consist of two formations, namely the coarse grained of alpine origin conglomerates cemented by calcareous clay and the fine grained, of marl, clay and sand.
- The Alpine formations of four geological zones, namely the flysch and limestones of the Tripolis zone, the limestones with chert intercalations and flysch of the Olonos-Pindos zone, the limestones and dolomites of Pelagonic and Parnasos zones. The limestones of the Pindos and Tripolis zone are characterized by the presence of a joint system, which favors infiltration of rainfall and karstification (Voudouris et al., 2005).

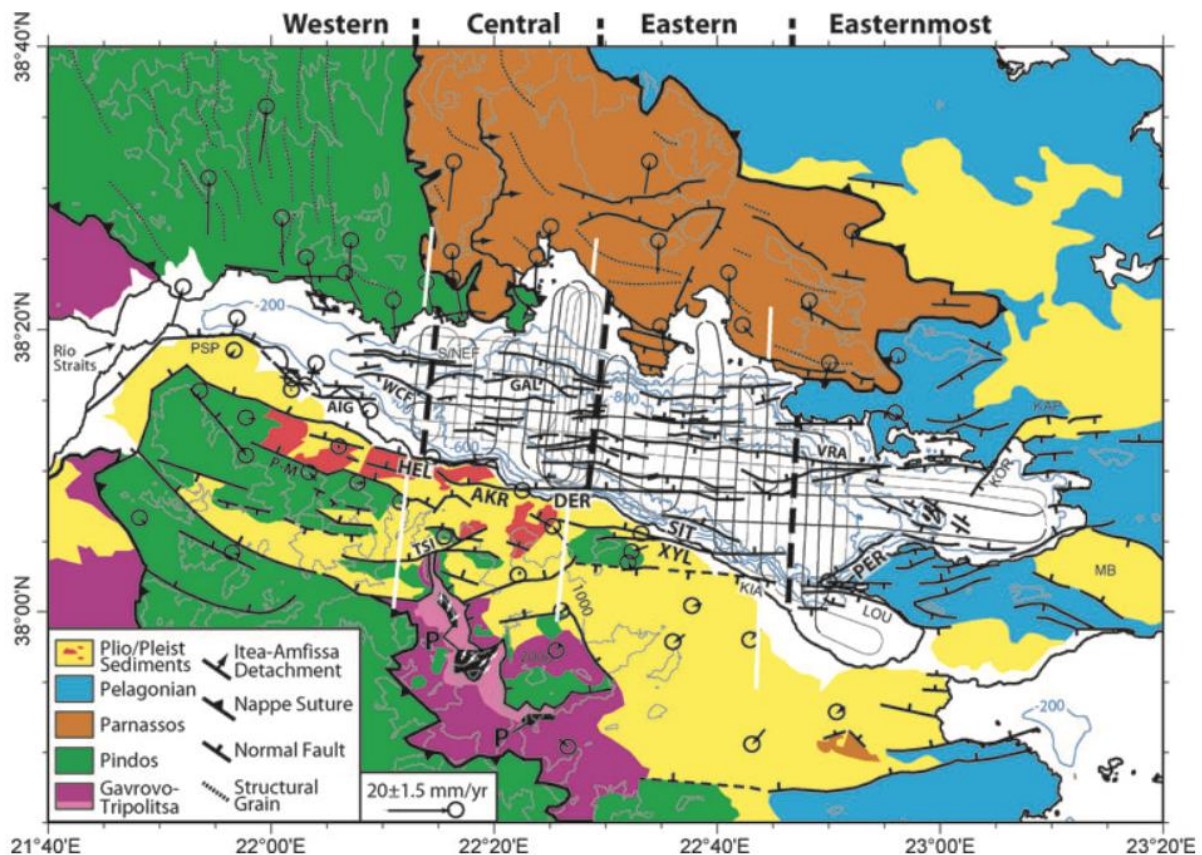


Figure 3.6: Geological formations map of Gulf of Corinth, in which the different geological zones are denoted with different colors in respect to the inset legend (after Taylor et al., 2011, and the references therein)

The complex geological structure of Gulf of Corinth results in a complicated hydrogeological setting, as well. The spatial distribution of the groundwater resources is nonhomogeneous. Voudouris et al. (2005) proposed three types of main groundwater aquifers. The first type consists of aquifers of the alluvial sediments. Alluvial aquifers are hosted in coastal areas and inland basins, supplying large quantities of water (light blue layers in Figure 3.7). The groundwater in the alluvium consists of phreatic and confined groundwater. The water table elevation is highest in April and lowest in October. Groundwater use on the coastal part exceeds natural recharge in dry period, and water levels decline to an extent that depends on the difference between abstraction and recharge. Groundwater flow approximately follows the surface drainage pattern. Overexploitation has caused a decline of groundwater levels in aquifer systems and changes in the direction and velocity of groundwater flow. The average hydraulic conductivity is equal to $k = 2 \times 10^{-4}$ m/sec as deduced from the conducted pumping test analyses (Voudouris, 1995; Koumantakis et al., 1999). The yield of boreholes ranges from 10-80 m³/h (Voudouris et al., 2005).

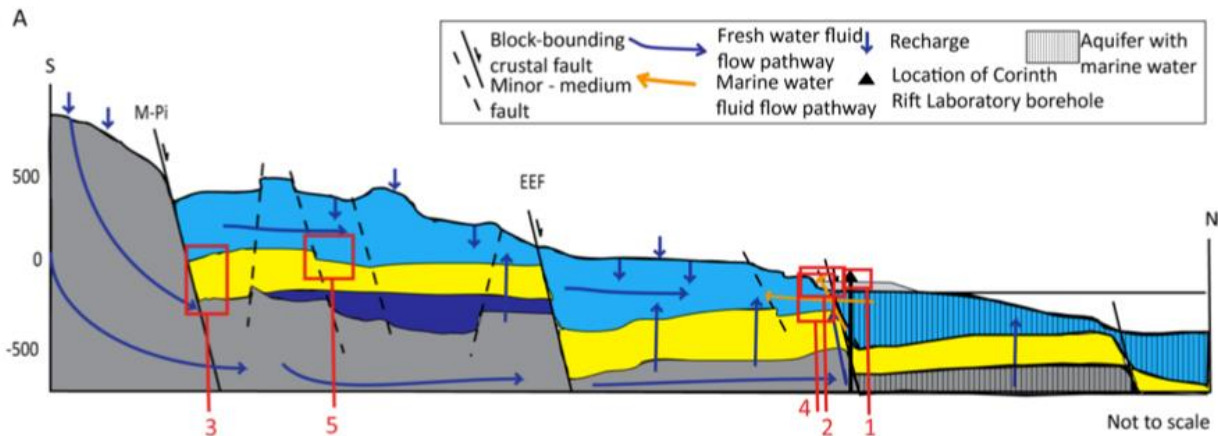


Figure 3.7: Schematic representation of the geology and the hydrogeology of the central-west southern flank of the Gulf of Corinth, showing the major aquifers (light blue, yellow and grey colors for the alluvial, Plio-Pleistocene and karstic type aquifers, respectively) and the possible fluid-flow pathways (after Rohais et al., 2007,2008; Ford et al., 2012; Loveless, 2013)

The second type of aquifers are the ones hosted in the Plio-Pleistocene sediments extended in the Gulf of Corinth (formations with yellow color in Figure 3.7), forming a multiple aquifer system (Giant Gilbert-type delta gravel conglomerate), which is at least 200 m thick. For example, the aquifer of Patras industrial area is the main aquifer for its groundwater. Analysis of pumping test data from boreholes drilled in Upper Pliocene conglomerates showed double porosity features and Transmissivity values between 45-62 m²/d (Voudouris et al., 2005). The last type of aquifers are the karstic ones, which are hosted in the carbonate rocks (limestones, dolomites), showing a high-water permeability due to its well-developed wide jointing (formations with grey color in Figure 3.7). The yield of boreholes ranges from 30 to 250 m³/h and Transmissivity varies between 50 and 950 m²/d (Voudouris, 1995). Karst aquifer systems often discharge groundwater through large springs. The locations of springs of the southern coastline of Corinth Gulf are shown in Figure 3.8.

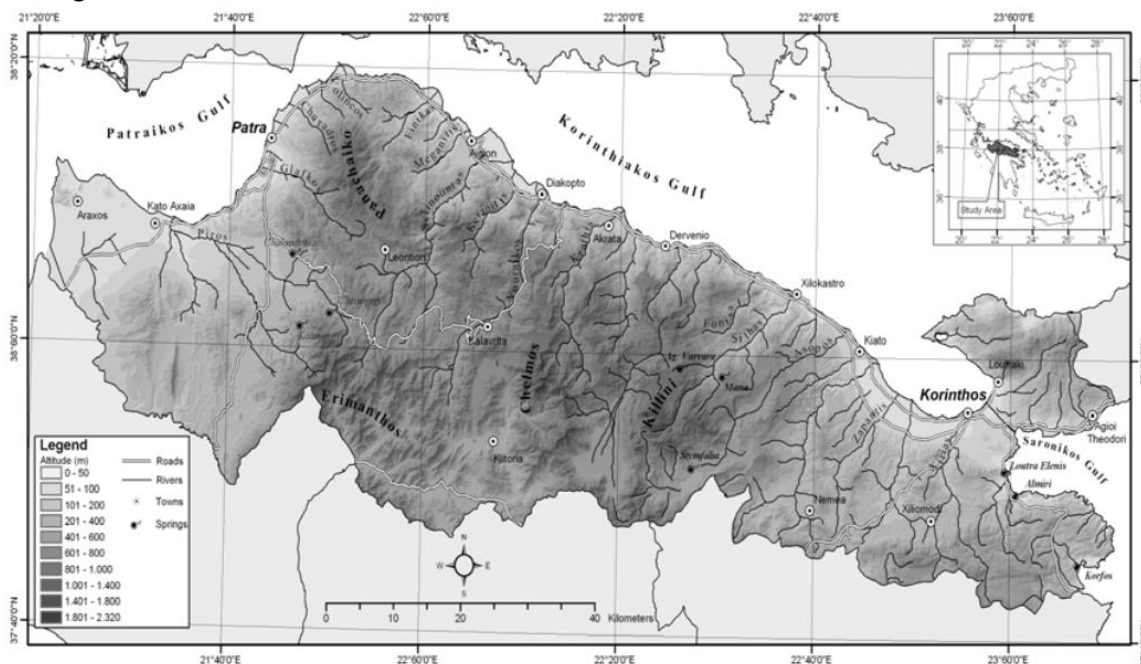


Figure 3.8: Location map of the south coastline of Corinth Gulf, showing geographical features and the location of its springs denoted with black circles (after Voudouris et al., 2005)

Seawater intrusion phenomena in karst aquifers have recorded in recent years, due to intensive exploitation. In the southeastern part of the area the karst aquifer is in direct hydraulic communication with the sea, contributing to sea water intrusion. A common feature in the karst system surrounding this area are solutions channels, which discharge water as submarine springs (Loutra Elenis, Almiros, Korfos). Based on geochemical and isotope data, Pizzino et al. (2004) suggest a dominantly meteoric origin of the groundwater. Recharge to the limestone aquifer occurs high in the Peloponnese Mountains to the south of the Gulf of Corinth, by direct rainfall, during the November to March wet season (Pizzino et al., 2004; Voudouris et al., 2005; Figure 3.7). They also hypothesized two topographically controlled circulation pathways; a quick, shallow circulation with local recharge in conglomerate and upper carbonate aquifers, and a longer, deeper circulation (flow path 5 to 10 km) in alkaline artesian aquifers (Pizzino et al., 2004; Giurgea et al., 2004; Micarelli et al., 2006).

Concerning the groundwater quality, its pH values are greater than 7 ($\text{pH} > 7$), indicating the slightly alkaline character of groundwater. Electrical conductivity is low in freshwater recharge area and progressively increases towards the coastline. In recharge areas the prevailing ions are Ca^{2+} and HCO_3^- . Moving seawards Na^+ , Cl^- , K^+ are the prevailing ions. The lowest concentration of sulfate occurs in groundwater from mountainous area. The waters are of various hydrochemical types: Ca- HCO_3 (freshwater of recent infiltration from mountainous area suitable for drinking), Na- HCO_3 (indicating ionexchange phenomena and characterizes a transition zone) and Na-Cl (typical brackish water from coastal aquifers affected by seawater intrusion).

The geochemical composition of groundwater in the southern rift flank is dominantly Ca- HCO_3 (Total Dissolved Solids $< 0.7 \text{ g l}^{-1}$), neutral to slightly alkaline and has a positive Eh (redox potential), thus should be oxidising (Pizzino et al., 2004). Calcite cement and iron oxide precipitates often found in sediment pores reflect these geochemical characteristics and can be used to delineate fluid-flow pathways. Based on geochemical and isotope data, Pizzino et al. (2004) suggest a dominantly meteoric origin of the groundwater. Recharge to the limestone aquifer occurs high in the Peloponnese Mountains to the south of the Gulf of Corinth, by direct rainfall, during November to March wet season (Pizzino et al., 2004; Voudouris et al., 2005). The Giant Gilbert-type delta gravel conglomerate aquifer is predominantly recharged by river flow (Voudouris et al., 2005). Groundwater of marine origin has been found in coastal conglomerates (Cornet et al., 2004). Pizzino et al. (2004) hypothesise two topographically controlled circulation pathways; a quick, shallow circulation with local recharge in conglomerate and upper carbonate aquifers, and a longer, deeper circulation (flow path 5 to 10 km) in alkaline artesian aquifers (Pizzino et al., 2004; Giurgea et al., 2004; Micarelli et al., 2006).

Unusually for such a rapidly rifting zone, no evidence has been found for hydrothermal activity across the southern flank of the Gulf of Corinth rift (Pizzino et al., 2004; Doan and Cornet, 2007; Pik et al., 2009). This anomaly has been attributed to masking of the expected thermal gradient by the strong topographic flow (Cornet et al., 2004; Pik et al., 2009), or extensive re-plumbing of the hydrogeological system caused by propagation of the Northern Anatolian Fault at $\sim 5 \text{ Ma}$ (Pik et al., 2009). However, groundwater geochemistry around several fault zones indicates flow of deeper waters (Pizzino et al., 2004; Pik et al., 2009).

Warm springs do exist in the Loutraki area, though geochemical data indicate that this is part of a waning, low enthalpy, geothermal system (Dotsika et al., 2010). Stamatis and Voudouris (2003) identify two aquifers across this region; an unconfined aquifer corresponding to delta conglomerates and recent alluvial sediment (up to 15 m thick), and sand beds of the Pliocene succession inter-bedded with, and confined by, marl. These have a total maximum thickness of 1000 m. Topographic flow is less significant across the more subdued topography of the Corinth Isthmus, east of the Lechaion Gulf.

Evidence from the Corinth Rift Laboratory reveal paradoxical hydrogeological behaviour of major basement faults. Regional aquifer connections allowing topographic flow from the Peloponnese Mountains to the coast are necessary to sustain the high water pressures experienced in the coastal aquifer (Figure 3.7). However,

the significant differences in measured pore pressures across the Aigion fault zone, and the separation of groundwater of marine origin in the hanging wall, from fresh groundwater in the footwall, indicates that these faults behave as major barriers (Cornet et al., 2004). This interpretation is supported by the presence of low permeability clay smearing and cementation along and adjacent to the fault zone (Cornet et al., 2004; Giurgea et al., 2004; Micarelli et al., 2006; Doan and Cornet, 2007). Hydraulic connections could result from spatial variations in fault zone properties, potentially enhanced by the high pressures in the lower aquifer (Giurgea et al., 2004), or by fluid-flow through relay zones at fault tips (Micarelli et al., 2006). Evidence indicative of the hydraulic behaviour of fault zones in the syn-rift sediment is limited, though geochemical evidence for mingled marine and meteoric groundwater in gravel conglomerates suggests fault zones do not prevent fluid-flow across them (Giurgea et al., 2004; Figure 3.7).

Voudouris et al. (2005) report a significant decrease in groundwater levels and saline intrusion since the 1980s due to over-abstraction of groundwater; demonstrating the sensitivity of groundwater resources in this arid climate. Nitrate contamination into aquifers from agricultural sources is also an issue across the region. In particular, there are concerns over the role of faults and their potential to behave as preferential fluid-flow pathways to contaminants (Stamatis and Voudouris, 2003; Giurgea et al., 2004; Voudouris et al., 2005).

3.3 References

- Cornet, F. H., Doan, M. L., Moretti, I., Borm, G., 2004. Drilling through the active Aigion Fault: the AIG10 well observatory. *CR Geosc.* 336, 395-406.
- Cushing, M., 1985. Evolution structurale de la marge nord-ouest hellénique dans l'île de Lefkada et ses environs (Grèce nord-occidentale). Ph. D. Thesis. Univ. de Paris-Sud (XI), Centre d'Orsay.
- Doan, M., Cornet, F.H., 2007. Thermal anomaly near the Aigio fault, Gulf of Corinth, Greece, maybe due to convection below the fault. *Geophys. Res. Lett.* 34, L06314.
- Dotsika, E. Poutoukis, D., Raco, B., 2010. Fluid geochemistry of the Methana Peninsula and Loutraki geothermal area, Greece. *J. Geoch. Explor.* 104, 97-104.
- Ford, M, Rohais, S., Williams, E.A., Bourlange, S., Joussetin, D., Backert, N., Malarte, F., 2013. Tectono-sedimentary evolution of the western Corinth rift (Central Greece). *Bas. Res.* 25, 3-25.
- Gaki-Papanastassiou, K., Karymbalis, E., Maroukian, H., Tsanakas, K., 2010. Geomorphic evolution of Western (Paliki) Kefalonia island (Greece) during Quaternary. *Bull. Geol. Soc. Greece* 43, 418-427.
- Gaki-Papanastassiou, K., Maroukian, H., Karymbalis, Papanastassiou, D., 2011. Geomorphological study and paleogeographic evolution of NW Kefalonia Island, Greece, concerning the hypothesis of a possible location of the Homeric Ithaca, in: Brown, A., Basell, L., Butzer, K. (Eds.), *Geoarchaeology, Climate Change, and Sustainability*. Geological Society of America Special Papers, 476, pp. 69-79.
- Giurgea, V., Rettenmaier, D., Pizzino, L., Unkel, I., Hötzl, H., Förster, A., Quattrocchi, F., 2004. Preliminary hydrogeological interpretation of the Aigion area from the AIG10 borehole data. *CR Geosc.* 336, 467- 475.
- IGME, 2010. Recording and evaluating of groundwater's hydrogeological characteristics and the aquifer system of Greece, 3rd Community Support Framework, Athens.
- Karymbalis, E., Papanastassiou, D., Gaki-Papanastasiou, K., Tsanakasm K., Maroukian, H., 2013. Geomorphological study of Cephalonia Island, Ionian Sea, Western Greece. *J. Maps* 9, 121-134. Doi: 10.1080/17445647.2012.758423.
- Katsafados, P., Kalogirou, S., Papadopoulos, A., Korres, G., 2012. Mapping long-term atmospheric variables over Greece. *J. Maps* 8. 181–184. [Doi:10.1080/17445647.2012.694273](https://doi.org/10.1080/17445647.2012.694273)

- Koumantakis I.E., 1989. Research of the aquifer system of Kefalonia Island: The regulation of the lake -spring of Megali Avuthos. Proposals for the exploitation of south-east Cephalonia Island. School of Mining and Metallurgy Engineering, Section of Geological Sciences, National Technical University of Athens. Greece.
- Koumantakis, J., Panagopoulos, A., Stavropoulos, X., Voudouris, K., 1999. Application of aquifer artificial recharge in the coastal alluvial basin of the northern part of Korinthos Prefecture, Proc. 5th Conf. on Hydrogeology, Nicosia, Cyprus, pp. 65-80.
- Loveless, S.E., 2013. The hydrogeological structure of fault zones in poorly lithified sediment, Gulf of Corinth rift. PhD Thesis. University of East Anglia, Norwich, United Kingdom.
- Micarelli, L., Moretti, I., Jaubert, M., Moulouel, H., 2006. Fracture analysis in the south-western Corinth rift (Greece) and implications on fault hydraulic behaviour. *Tectonophysics*, 426, 21-59.
- Papathanasiou, G., Valkaniotis, S., Ganas, A., Grendas, N., Kollia, E., 2017. The November 17th, 2015 Lefkada (Greece) strike-slip earthquake: Field mapping of generated failures and assessment of macroseismic intensity ESI-07. *Eng. Geol.* 220, 13-30. [Doi:10.1016/j.enggeo.2017.01.019](https://doi.org/10.1016/j.enggeo.2017.01.019)
- Pik, R., Marty, B., 2009. Helium isotopic signature of modern and fossil fluids associated with the Corinth rift fault zone (Greece): Implication for fault connectivity in the lower crust. *Chem. Geol.* 266, 67-75.
- Pizzino, L., Quattrocchi, F., Cinti, D., Galli, G., 2004. Fluid geochemistry along the Eliki and Aigion seismogenic segments (Gulf of Corinth, Greece). *CR Geosc.* 336, 367-374.
- Rohais, S., Eschard, R., Ford, M., Guillocheau, F., and Moretti, I. 2007. Stratigraphic architecture of the Plio-Pleistocene infill of the Corinth Rift: Implications for its structural evolution. *Tectonophysics* 440 (1–4). 5-28.
- Rohais, S. Eschard, R., Guillocheau, F., 2008. Depositional model and stratigraphic architecture of rift climax Gilbert-type fan deltas (Gulf of Corinth, Greece). *Sediment. Geol.* 210, 132-145.
- Rondoyanni, Th., Mettos, A., Paschos, P., Georgiou, Ch., 2007. Neotectonic map of Greece, scale 1:100.000, Lefkada sheet. I.G.M.E., Athens.
- Sazakli, E., Alexopoulos, A., Leotsinidis, M., 2007. Rainwater harvesting, quality assessment and utilization in Kefalonia Island, Greece. *Water Res.* 41, 2039-2047.
- Special Secretariat for Water, 2014. Management plan of the river basins of western Sterea Ellada river basin district. Ministry of Environment, Energy and Climate Change, Athens, Greece.
- Stamatis, G., Voudouris, K., 2003. Marine and human activity influences on groundwater quality of Southern Korinthos area (Greece). *Hydrol. Process.* 17, 2327-2345.
- Stefouli, M., Vasiliou, E., Charou, E., Stathopoulos, N., Perrakis, A., Giampouras, P., 2013. Remote sensing techniques as a tool for detecting water outflows. The case study of Cephalonia Island. *Bull. Geol. Soc. Greece* 47, 1519-1528.
- Taylor, B., Weiss, J.R., Goodliffe, A.M., Sachpazi, M., Laigle, M., Hirn, A., 2011. The structure, stratigraphy and evolution of the Gulf of Corinth rift, Greece. *Geophys. J. Int.* 185, 1189-1219.
- Voudouris, K., 1995. Hydrogeological conditions in NW Achaia. Ph. D. Thesis. University of Patras, Patra, Greece.
- Voudouris, K., Daskalaki, P., Antonakos, A., 2005. Water resources and groundwater quality in Northern Peloponnesus (Greece). *G-NEST*, 7(3), 340-353.

4 Hydrogeology of Bedretto lab and Swiss Alps

This section aims at describing the hydrogeology of the Swiss Alps and the Bedretto Lab. First, an overview on the hydrogeological conditions of Switzerland is given, followed by an overview on the hydrogeology of the Bedretto Lab.

4.1 Hydrogeology of the Swiss Alps

Due to its topography and related climate, water is abundant in Switzerland. The sources of large rivers that flow to the Northern Sea (Rhine), the Mediterranean Sea (Rhône), and the Black Sea (Inn, transforming into the Donau) are located in the Swiss Alps.

The hydrogeology of Switzerland is complex due to the topographic and geological diversity. Each rock type has unique characteristics that affect the flow and storage of water. In general, the permeability decreases with depth (e.g. Ingebritsen et al. 2006). In Switzerland, the hydrogeologic conditions can be assigned basically to three types of aquifers: i) Unconsolidated aquifers, ii) fissured aquifers, and iii) Karst aquifers. Each of these types has a different behaviour regarding flow velocity, storage capacity, and water in- and exfiltration (e.g. Sinreich, 2012, Kozel 2013).

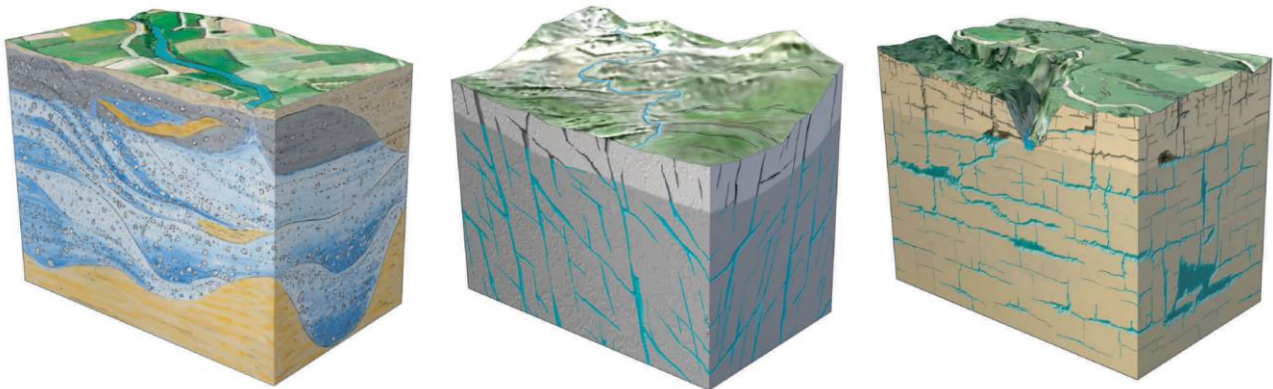


Figure 4.1: Aquifer types in Switzerland. Left: unconsolidated aquifer, middle: fissured aquifer, right: Karst aquifer (Figure from Sinreich 2012)

Unconsolidated aquifers occur along large rivers and in Alpine valleys, where sediment-filled troughs exist. Such aquifers generally have a high storage capacity. Their typical hydraulic conductivities (dependent on grain size) range between $K=10^{-5}$ to 10^{-2} m/s (Tripet 2005) and references therein). Aquifers in the Alps are mainly fissured, i.e. the water flows mainly along fissures and partly through the pores of the rocks. Flow velocities are mainly dependent on the width of the fissures and their connectedness. They range between few and several 100 m per day (Tripet 2005). In the Jura-region (NW Switzerland) and in some parts of the Alps, Karst aquifers dominate. As Karst systems are rich in cavities, groundwater can flow fast in such aquifers, with velocities of several tens of m/s (Tripet 2005). (Fig. 4.2).

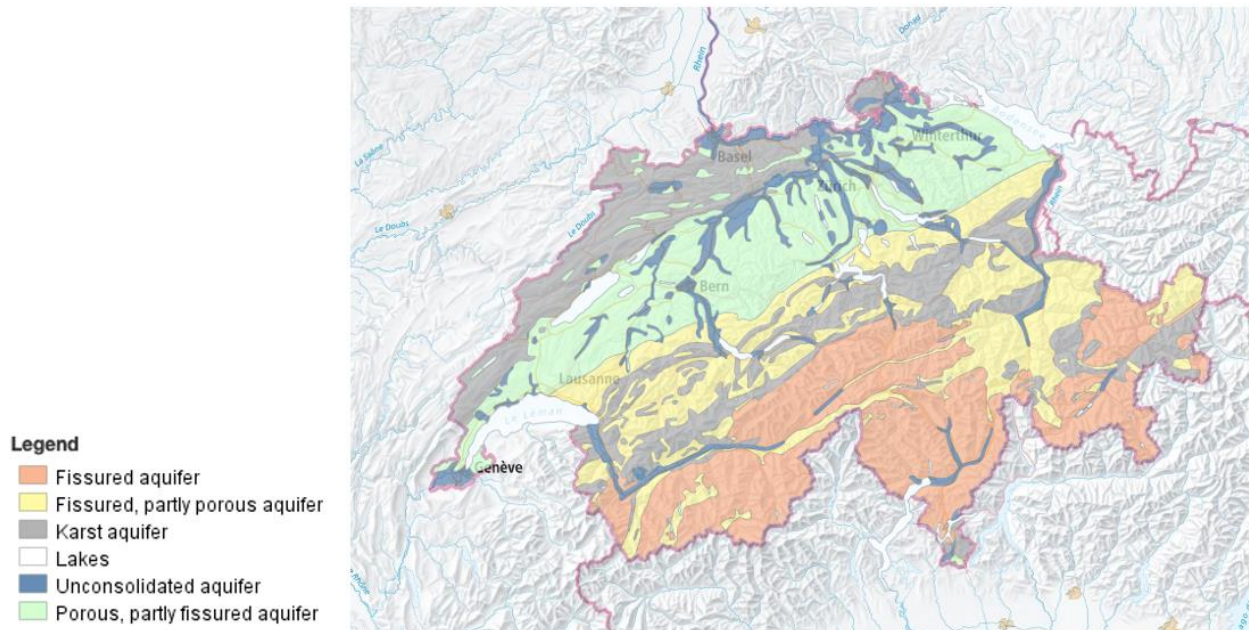


Figure 4.2: Hydrogeological Overview of Switzerland (data: BAFU 2023)

Switzerland is rich in groundwater: around 150 km³ of water is available in the country's underground. The largest part (120 km³) of groundwater is stored in Karst aquifers, whereas fissured (20 km³) and unconsolidated aquifers (10 km³) only contribute minor parts (Sinreich et al., 2012). The build-up of groundwater depends on many factors, including as topography, soil type and climatic factors. With depth, temperature generally increases (ca. 3°/100 m depth), therefore the deep groundwater can be used as energy source.

The 1:500000 hydrogeological map of Switzerland provides qualitative estimates of the yield of different aquifer types (Schürch et al. 2007). The map reflects the strong relation between geology, surface water, and ground water.

Following an earthquake, various processes that change hydrogeologic properties, may occur, investigated by the field of Earthquake Hydrology. Earthquakes cause strain, which changes fluid pressures and alters hydrogeologic properties, including permeability, which controls the fluid-flow rate (e.g. Manga and Wang, 2015). Hence, it is crucial to have an overview of the hydrogeologic characteristics of the investigation area.

4.2 Hydrogeology of the Bedretto site

Previous studies (Offerdinger, 2001; Offerdinger et al. 2014) have shown that the groundwater sampled in the Bedretto lab has a meteoric origin with a major contribution from glacial melt water. Three major glaciers are located in the region of the Bedretto tunnel, which are the Geren glacier, the Witenwasserenglacier, and the Mutten glacier. No indications of upwelling brines or convection driven flow are observed. The waters that reach the tunnel have very short transit times, as their age has been determined (in the northwestern tunnel section) to 1 to 1.5 years.

Tables with hydraulic conductivities at several sections of the Bedretto Tunnel can be found in Offerdinger et al. (2014). The spatial average groundwater recharge rate for the area is 12.05×10^{-4} m/day (i.e. ~1 mm /day).

As the structural features mainly strike perpendicular to the tunnel, fluid flow follows that orientation. Fluid flow is not uniform in the Rotondo granite and alternates between dripping zones and zones of continuous

inflow (Arnet 2021 and References therein). The highest inflows (up to 130 l/s) occur between TM 300 and 400, at TM 1300 to 1400, at TM2800 to 2900, and at TM 4200 to 4300 (Masset & Loew, 2010).



Figure 4.3 Example of water sampling from a) a fracture zone and b) a borehole (Photos: M. Strupler)

Water is being sampled and analyzed for various parameters at different fracture zones and boreholes, including Temperature, pH, Electric conductivity, flow rate, major ions, stable water isotopes. For details, see Arnet (2021).

The mean fluid inflow temperatures at the fracture zones of the Bedretto Tunnel vary between 5 and 19.5°C. Temperatures generally increase with distance from the tunnel entrance, with negative temperature anomalies at zones of high inflows (TM 1300, TM2850, and TM4300) (Arnet 2021). Temperatures of the borehole water ranges between 16.8 and 20°C.

The pH of the water samples taken at the fractures in the tunnel averages around 9. In the open boreholes, pH is slightly higher (between 9 and 10). The discharge rate at various fractures in the tunnel range between a few ml/s and 2.5l/s. At the boreholes it ranges between 0.1 and 0.2 ml/s (Arnet 2021).

Long time series of observations are needed in order to better investigate the various dependencies of the parameters. Due to the little fluctuations in temperature and air pressure, the Bedretto Lab offers prime conditions for measuring radon time series.

4.3 References

Arnet, M., 2021. Deep Alpine Fluids: Origin, pathways and dynamic remobilisation in response to hydraulic stimulations at the Bedretto Underground Laboratory for Geoenergies (BULGG) Master's Thesis, ETH Zurich. <https://doi.org/10.3929/ethz-b-000532915>

BAFU 2023. Übersichtskarte Hydrogeologie. URL <https://www.bafu.admin.ch/bafu/de/home/zustand/daten/geodaten/wasser--geodaten.html> (accessed: 27.04.2023)

Ingebritsen, S. E., Sanford, W. E., Neuzil, C. E., 2006. Groundwater in geologic processes, 2nd edition. Cambridge University Press. <http://pubs.er.usgs.gov/publication/70178403>

Kozel, R., 2013. Grundwasser in der Schweiz. Aqua Viva, 10–15.

Manga, M., Wang, C.-Y., 2015. Earthquake Hydrology. In G. Schubert (Ed.), Treatise on Geophysics, 2nd ed., Vol. 4, pp. 305–328. Elsevier. <https://doi.org/10.1016/B978-0-444-53802-4.00082-8>

Ofterdinger U.S., 2001. Groundwater flow systems in the Rotondo Granite, Central Alps (Switzerland). PhD thesis, Swiss Federal Institute of Technology (ETH) Zurich, Switzerland.

Ofterdinger, U. S., Renard, P., Loew, S., 2014. Hydraulic subsurface measurements and hydrodynamic modelling as indicators for groundwater flow systems in the Rotondo granite , Central Alps (Switzerland). 278(November 2012), 255–278. <https://doi.org/10.1002/hyp.9568>

Schürch, M., Kozel, R., Jemelin, L. 2007. Hydrogeological mapping in Switzerland. Hydrogeology Journal, 15(4), 799–808. <https://doi.org/10.1007/s10040-006-0136-y>

Sinreich, M., Kozel, R., Lützenkirchen, V., Matousek, F., Jeannin, P.-Y., Löw, S., Stauffer, F., 2012. Grundwasserressourcen der Schweiz. Abschätzung von Kennwerten. Aqua & Gas, 9, 16–28.

Tripet J.P., 2005. Grundwasser. In: Spreafico M., Weingartner R. (Hrsg.) Hydrologie der Schweiz – Ausgewählte Aspekte und Resultate. Berichte des BWG, Serie Wasser Nr. 7. Bern: 79–100.